Sensitivity and optimality analysis of breathing scenarios for 1D or 0D models of gas diffusion in the lung

Céline Grandmont, Cyril Karamaoun, Sébastien Martin, Frédérique Noël

SENSITIVITY AND OPTIMALITY ANALYSIS OF BREATHING SCENARIOS FOR 1D OR 0D MODELS OF GAS DIFFUSION IN THE LUNG

CÉLINE GRANDMONT[1], CYRIL KARAMAOUN[2], SÉBASTIEN MARTIN[3], AND FRÉDÉRIQUE NOËL[4]

Abstract. In the present work we propose a new nonlinear coupled 1D model to describe lung ventilation and the transport and diffusion of both oxygen and carbon dioxide in the bronchial tree through the blood. It takes into account the *so-called* Bohr-Haldane effect, which induces a strong coupling of oxygen and carbon dioxide, and is driven by the applied pleural pressure. The ability of this model to reproduce standard acknowledged values in healthy situations and normal breathing scenario is provided. One key aspect is that, contrary to its 0D counterpart, it naturally takes into account mixing of gases along the tree and a time delay as the gases have to be transported before reaching the alveoli. We investigate the sensitivity of the 1D model to model parameters, its behavior at exercise and recover standard washout carbon dioxide curves. We also investigate the sensitivity of both the 1D model and its 0D counterpart with respect to the breathing pattern by considering two types of pleural applied pressure: a piecewise constant one and a piecewise exponential one for various values of the breathing period, inspiratory ratio and pressure amplitude. We finally explore which cost functions the observed stereotypical breathing scenario for normal breathing in healthy situations may optimize, emphasizing the fact that it should be a combination of several criteria: low effort and small lung distension while maintaining average carbon dioxide arterial partial pressure at a given level. The paper concludes with a discussion on the proposed model, its limitations and further works.

1. Introduction

The primary function of the lungs is to transport air through breathing cycles, from the external environment into the acini, where gas exchange occurs via diffusion of oxygen and carbon dioxide into and out of the blood. This diffusion process couples the dynamics of oxygen and carbon dioxide, as hemoglobin affinity depends on both pH and the partial pressure of carbon dioxide in the blood. Mathematical modeling of this integrated system can provide major insights into lung function, both in health and disease. Depending on the physiological phenomena under study and the available data, different models can be developed − ranging from macroscopic models that describe, for instance, the time evolution of global quantities [1, 3, 4, 10, 15, 39] to multiphysics and multiscale models that capture multidimensional lung mechanics [6, 18, 19, 34, 35, 42], airflow [2, 12, 14] and gas diffusion [24]. A common feature of all these models is that they aim to provide either a strong general framework or high predictive accuracy [26].

The so-called 0D models are based on a simplified representation of the lungs, with time dependency and no explicit spatial dimension. The simplest model to describe ventilation is the single balloon model, where a rigid tube – the bronchial tree – is connected to an inflatable elastic balloon, i.e., the alveoli [3]. More complex 0D models have been proposed, taking into account various physiological phenomena [1, 4, 10, 15, 39] and thus possibly involving a large number of parameters, making their fitting and use for understanding dominant phenomena challenging. Moreover, because they do not include any spatial dimension, they are not well suited, *per se*, for studying transport phenomena such as the transport of gases in the bronchial and alveolar compartments. Note that transport induces a time delay that has to be modelled and calibrated for 0D models to be accurate, particularly when modeling the control of respiration [1, 10, 15, 39]. Dimensional models have been explored to tackle these issues. Full 3D models of the lungs can provide numerical simulations of air transport [2, 12, 14], lung mechanics [34] or multiscale coupled airflow and parenchyma deformation

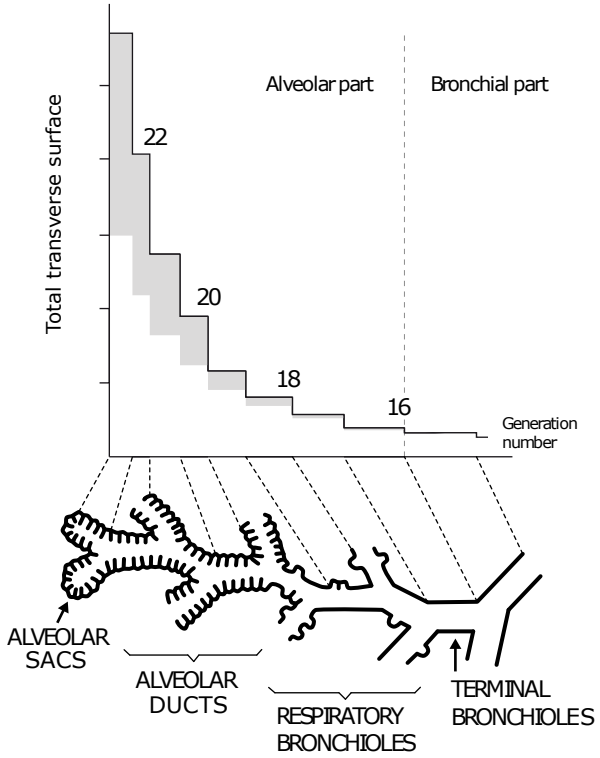

FIGURE 1. Trumpet. Light grey: alveolar part. Adapted from [21]

models [6, 18, 19, 35, 42]. Yet, simulations in 3D geometries require medical imaging data and imply high computational costs. Moreover, they are adapted to patient specific issues but may be less adaptable for understanding overall function. An intermediate approach is possible. One or two-dimensional models are based on key symmetry assumptions of the lung structure. This allows for introducing spatial dimensions in the models and consider some heterogeneities while keeping the complexity and the simulation cost low. Among these models, the 1D approach [24, 29, 33] is based on the approximation that each bronchus is a perfect cylinder with identical dimensions at each level of bifurcation of the bronchial tree. In essence, this strong hypothesis allows for the aggregation of all bronchi of the same level of subdivision, i.e., generation, in a single tube whose transverse surface corresponds to the sum of the transverse surface of each bronchus in this generation (see Section 2.1 for detailed modeling). This leads to a characteristic *trumpet-shaped* model of the bronchi and alveoli, with a dominant axial dimension and increased cross-sectional surface along the generations (see Fig. 1) as the number of bronchi increases exponentially at each level of subdivision. These models enable the description of the airflow as well as the transport and diffusion of oxygen [24] and carbon dioxide [29]. They can be used to simulate gas mixing along the bronchial tree, understand the impact of the breathing scenario, and explain why one observes stereotypical scenarios for normal breathing [29].

Mechanically, the primary objective of breathing is to reduce the work involved and the mechanical elongation in the bronchi, while, physiologically, it aims to sustain and regulate the amount of oxygen and carbon dioxide in the blood. Hence, the regulation of ventilation is governed, thanks to chemical sensors, by the levels of arterial pressure for oxygen (P_{a,O_2}) and carbon dioxide (P_{a,CO_2}) with P_{a,CO_2} serving as the most vital regulator [16, 22]. To keep P_{a,CO_2} near 40 mmHg, which is the carbon dioxide partial pressure in the oxygenated blood, both the breathing rate and the depth of each breath are carefully controlled [22]. Different models of the control of breathing have been developed in the literature in order to recover the stereotypical breathing parameters observed in

physiology. Among those, two different approaches have appeared: feedback control and optimal control. On one hand, the feedback control approach often relies on complex ODE systems that take into account not only the ventilation and gas diffusion but also other parts of the body. In [15], gas concentrations in the tissues and the brain are considered; in [39], the consumption of muscles is further added, and in [10], the respiratory system, the central nervous system, and the cardiovascular system are modelled. In these studies, one crucial issue is to accurately model the time delay coming in particular from the transport phenomena and thus to fit the various delay times appearing in the whole system. On the other hand, the optimal control approach is based on minimizing of the work of breathing [29, 31] or the average respiratory muscle force [27] (or even both [17]) while satisfying a constraint on the amount of oxygen exchanged with the blood [29] or the alveolar ventilation rate [27, 31]. It focuses only on the respiratory system and on the exchanges made with the blood.

Our aim here is to propose a dynamical model able to describe the ventilation and gas diffusion processes of both oxygen and carbon dioxide that take into account transport phenomena along the bronchial tree. One main issue is to describe the *so-called* Bohr-Haldane effect [49] which induces a strong coupling between oxygen and carbon dioxide blood partial pressures. With this model at hand, our second goal is to explore which quantities control the breathing cycle: indeed, as already stated, the role of the lung is to ensure the oxygen transfer from the outside air to the blood and the carbon dioxide transfer from the blood to the outside air while maintaining oxygen and carbon dioxide blood partial pressures at given levels. To achieve this, the breathing pattern has to adapt, and a key question is which quantities it optimizes. The same issues have been tackled in [29], yet with some main differences compared to what we propose herein. Here, the breathing cycle is driven by an applied pressure (not a given flux as in [29]), the proposed 1D model is based on morphometric data, includes mass-flow conservation of the gases, and the diffusion process includes the Bohr-Haldane effect. Consequently, the proposed model is able to recover standard breathing quantities, without any fitting of the physiological parameters, in healthy situations at rest and during exercise together with carbon dioxide washout curves. Moreover, in [29], the proposed cost function is the work of breathing with a given oxygen flux constraint. Here, we focus on different cost functions involving the work of breathing, the arterial partial pressure of carbon dioxide, and lung distension. These choices are motivated by physiological considerations: the need to avoid patient fatigue, and the existence of lung tissue elongation and blood carbon dioxide partial pressure sensors [16, 22].

More precisely, we

- present a model that takes gas transport into account by connecting a 1D geometrical model of the bronchial tree [24] to the breathing dynamics characteristic of a 0D model [26]. This connected model is enriched by a recent dynamical model of alveolar gas exchange, taking into account the interaction between oxygen and carbon dioxide in the blood [7]. This model provides concentrations of oxygen and carbon dioxide along the bronchial tree, fluxes of these gases through the alveolar-capillary membrane, and their blood partial pressures.
- compare our new full model to the 0D model developed in [7] pointing out the transport time delay phenomena.
- explore the impact of the breathing scenario (modifying the applied pressure), and investigate the dependencies with respect to inspiratory pressure, frequency, and inspiratory ratio.
- investigate whether standard breathing minimizes work or the variations in lung volume compared to the functional residual capacity V_{FRC} while maintaining the carbon dioxide partial pressure in the arterial blood $\mathrm{P}_{a,\mathrm{CO}_2}$ as close as possible to 40 mmHg, in order to understand which criteria are optimized by the breathing pattern observed in practice.

The paper ends with a discussion section on the model, comparing it to other existing models and highlighting its limitations and possible extensions for clinical purposes.

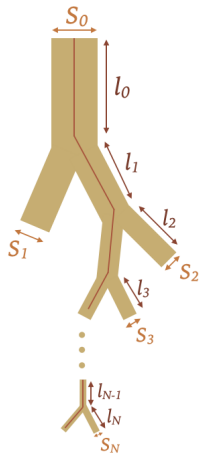

FIGURE 2. Modeling of the human lung. A bronchus of generation i is characterized by its length l_i and section area S_i, built upon morphometrical data. Each bronchus divides into two daughter bronchi.

2. METHODS

2.1. **Morphometric 1D model of the lung.** The lung is modelled as a symmetric dichotomic bifurcating tree composed of N generations (see Fig. 2). Typically, there are around $N = 24$ generations in the human lung, numbered from $g = 0$ (trachea) to $g = 23$. The lung can then be divided into two parts, the bronchial tree, which consists of the first 16 generations, and the acini, where the exchange with the blood takes place, which comprise the last 8 generations [33, 45, 48].

Each bronchus of a generation g is then represented by a cylinder with a length l_g and a radius r_g. We can then define what we call the length of the lung, L, which corresponds to the length of a path going from the trachea to the last generation of the tree:

$$L = \sum_{g=0}^{N-1} l_g. \tag{1}$$

We introduce $L_k := \sum_{g=0}^{k} l_g$, the path length from the entrance of the trachea to the end of a bronchus of generation k. It means that a bronchus of generation g is located along the path length within $\{x \in (L_{g-1}, L_g)\}$, with $L_{-1} = 0$. Let us now introduce lineic quantities related to the path length.

- ***Bronchial volume and lineic bronchial volume.*** The airway cross-section and volume of the 2^g cylinders of generation g are $S_g := 2^g \pi r_g^2$ and $V_g := 2^g \pi r_g^2 l_g$, respectively. This allows us to define the lineic volume of the bronchial tree as

$$\tilde{V}_b(x) := \sum_{g=0}^{23} \frac{V_g}{l_g} \mathbf{1}_{(L_{g-1}, L_g)}(x), \tag{2}$$

which corresponds to the airway cross-section along the path: as the volumes are made of ducts, the lineic volume distribution simply reads as the piecewise constant function (on each generation), equal to the airway cross section, and thus $\tilde{V}_b(x) = S(x)$ with

$$S(x) = \sum_{g=0}^{23} S_g \mathbf{1}_{(L_{g-1}, L_g)}(x).$$

The total bronchial volume V_b is equal to $\displaystyle\int_0^L \tilde{V}_b(x)\,\mathrm{d}x = \sum_{g=0}^{23} V_g$.

- ***Alveolar surface area and lineic alveolar surface area.*** The total alveolar surface at rest is set to $\Sigma = 120\,\mathrm{m}^2$ and, as in [49, 38], we distribute the corresponding surface only in the acinar region, i.e., from generation 16 to 23, as follows: the alveolar surface area is distributed to the different generations in proportion to the duct surface $2^g \times 2\pi r_g \times l_g$. This provides the distribution of alveolar area $g \mapsto \Sigma_g$ such that, on the one hand, $\Sigma_g = 0$ for $g \in \{0, \cdots, 15\}$ as the generations from 0 to 15 are not alveolated and, on the other hand, $\Sigma = \sum_{g=0}^{23} \Sigma_g$. This allows us to define the *lineic surface area of alveoli* as

$$\tilde{\Sigma}(x) = \sum_{g=0}^{23} \frac{\Sigma_g}{l_g} \mathbf{1}_{(L_{g-1}, L_g)}(x). \tag{3}$$

  Noteworthily, multiplying by the function $x \mapsto \frac{\tilde{\Sigma}(x)}{\Sigma}$ allows us to convert any surface area at time t into a lineic surface area, in accordance with the alveolar surface area distribution determined at rest.
- ***Alveolar volume and lineic bronchial volume.*** As for the alveolar surface area, we define $\Omega_g := (\Sigma_g)^{\frac{3}{2}}$ and $\Omega := \sum_{g=0}^{23} \Omega_g$. This allows us to define

$$\tilde{\Omega}(x) = \sum_{g=0}^{23} \frac{\Omega_g}{l_g} \mathbf{1}_{(L_{g-1}, L_g)}(x).$$

  Noteworthily, multiplying by the function $x \mapsto \frac{\tilde{\Omega}(x)}{\Omega}$ allows us to convert any total alveolar volume at time t into a lineic alveolar volume, in accordance with the alveolar volume distribution determined at rest: for a given alveolar volume at time t $V_a(t)$, the lineic alveolar volume is defined as

$$\tilde{V}_a(t,x) := \frac{\tilde{\Omega}(x)}{\Omega} V_a(t).$$

  By construction, $\tilde{V}_a$ and V_a are related by $V_a(t) = \displaystyle\int_0^L \tilde{V}_a(t,x)\,\mathrm{d}x$.

Let us now consider the lung volume $V(t)$ at time t: this volume will be the solution to a 0D mechanical model. The total volume is divided into two contributions: the bronchial volume, denoted V_b, which is defined by the morphometry and assumed to be time-independent, and the alveolar volume, denoted $V_a(t)$, which corresponds to $V(t) - V_b$. Then, the lineic volumes are given by

$$\tilde{V}_a(t,x) := \frac{\tilde{\Omega}(x)}{\Omega}(V(t) - V_b), \qquad \tilde{V}(t,x) := \tilde{V}_b(x) + \tilde{V}_a(t,x), \tag{4}$$

with $\tilde{V}_b$ defined by (2). By construction, we have

$$V_b = \int_0^L \tilde{V}_b(x)\,\mathrm{d}x, \qquad V_a(t) = \int_0^L \tilde{V}_a(t,x)\,\mathrm{d}x, \qquad V(t) = \int_0^L \tilde{V}(t,x)\,\mathrm{d}x.$$

2.2. **0D mechanical model of ventilation.** In order to compute the evolution of the volume of the lung and the airflow through the lung, we use a well-known mechanical model that assumes that the lung can be considered as a resistive tube representing the bronchial tree linked to an elastic balloon representing the acinus [7, 26]. This model is written as

$$-P(t) = E(V(t) - V_{\mathrm{FRC}}) + R\dot{V}(t), \tag{5}$$

where $P(t)$ is the pleural pressure during spontaneous breathing, E is the elastance of the lung, V is the volume of the lung, V_{FRC} is the functional residual capacity (namely, the lung volume at the end of a passive expiration), and R is the resistance of the lung (that accounts for the resistance of bronchial tree and tissue viscosity).

Thanks to this model, we can compute the lung volume $V(t)$ and, as a consequence, the alveolar lineic volume $\tilde{V}_a(t,x)$, and the total lineic volume $\tilde{V}(t,x)$. Note that, as we assume that the bronchial tree does not expand in time, the lineic bronchial volume is computed only once and does not evolve in time: $\tilde{V}_b(x) = S(x)$.

2.3. **Transport of the gases in the tree.** To model the transport of the respiratory gases in the tree, we assume that the displacement of each gas is homogeneous across a cross section S_g. It allows us to model the transport of the respiratory gases with a one dimensional model that goes from $x = 0$ the entrance of the trachea to $x = L$ the end of the last generation of the acinus.

In our model, considering that air in the lung is incompressible as in [24], the time variation of the total lineic volume of the lung is equal to the flux of the fluid velocity across a section. It can be written as

$$\partial_t \tilde{V} + \partial_x(Su) = 0, \text{ in } (0,L), \tag{6}$$

where $\tilde{V}$ is the total lineic volume defined by (4) and u is the velocity of the air. In the equation of the conservation of air volume, our only unknown is u the velocity of the air along the tree (the volume $\tilde{V}$ defined by (4) is known from V obtained by solving the mechanical equation (5)). This velocity is obtained by integrating in space equation (6), using the boundary condition

$$S(0)u(t,0) = \dot{V}, \quad \text{during inspiration,}$$

and

$$S(L)u(t,L) = 0, \quad \text{during expiration.}$$

Next, we assume that the transport of the respiratory gases in the tree is mainly due to convection and diffusion. A reaction term models the exchange occurring with the blood in the acinus. This results in the following coupled equations for the oxygen and carbon dioxide

$$\partial_t(\tilde{V}\chi_{\mathrm{O_2}}) + \partial_x(Su\chi_{\mathrm{O_2}}) - D_{\mathrm{O_2}}\partial_x(S\partial_x\chi_{\mathrm{O_2}}) = -\frac{\tilde{\Sigma}}{\Sigma}\dot{V}_{\mathrm{O_2}}(\chi_{\mathrm{O_2}}, \chi_{\mathrm{CO_2}}), \text{ in } (0,L), \tag{7}$$

$$\partial_t(\tilde{V}\chi_{\mathrm{CO_2}}) + \partial_x(Su\chi_{\mathrm{CO_2}}) - D_{\mathrm{CO_2}}\partial_x(S\partial_x\chi_{\mathrm{CO_2}}) = -\frac{\tilde{\Sigma}}{\Sigma}\dot{V}_{\mathrm{CO_2}}(\chi_{\mathrm{CO_2}}, \chi_{\mathrm{O_2}}), \text{ in } (0,L), \tag{8}$$

where χ_{gas} corresponds to the mole fraction of the considered gas, D_{gas} is the diffusion coefficient of the considered gas in the air and $\dot{V}_{\mathrm{gas}}(\chi_{\mathrm{gas}}, \cdot)$ corresponds to the amount of gas exchanged with blood: note that, due to the Bohr-Haldane effect, gas exchanges of O_2 and CO_2 at the alveolar-capillary membrane involve a coupling in the dynamics of O_2 and CO_2 in the bloodstream, hence in the flux of gases that pass through the membrane. Due to this, equations (7) and (8) are strongly coupled. This was not the case in [24] which considers only the dynamics of O_2 nor in [29] where the source term of the oxygen part was independent of the carbon dioxide. We complete this set of equations with initial conditions χ^0_{gas} and with boundary conditions depending also on the breathing cycle, namely

- At inspiration,
$$\chi_{\mathrm{gas}}(t,0) = \overline{\chi}_{\mathrm{gas}}, \qquad \partial_x\chi_{\mathrm{gas}}(t,L) = 0.$$
Here the Dirichlet boundary condition at $x = 0$ implies that the bronchial tree is supplied with fresh air in which the considered gas has a fraction $\overline{\chi}_{\mathrm{gas}}$, namely 0.21 for O_2 and 0.04 for CO_2 (these values could be modified according to the specific environment, for instance in the case of artificial oxygen supply). The Neumann boundary condition at $x = L$ means

that the total flux (advective+diffusive) is zero at the tree terminals (note that the advective flux is zero as well, as the air velocity at the tree terminals is zero).

- At expiration,

$$\partial_x \chi_{\text{gas}}(t,0) = 0, \qquad \partial_x \chi_{\text{gas}}(t,L) = 0.$$

This means that the flux leaving the tree at the mouth is purely advective, whereas the Neumann boundary condition at the tree terminals remains the same as in the inspiration regime.

Let us emphasize that the boundary conditions for the reaction-advection-diffusion equation change from inspiration to expiration.

2.4. **Exchange of respiratory gases between alveoli and blood.** Let us first describe the transfer dynamics between the blood and the alveoli as in [7]. We assume that a volume V_c of blood is brought near the acinus where the exchange can occur. It remains in the neighbourhood for a transient time τ_b. The capillary volume of blood V_c is then removed and replaced by a new volume V_c of blood. This results in the following dynamics for the gas concentrations, for $\theta \in [0, \tau_b]$,

(9)
$$\begin{cases} V_c \frac{\mathrm{d}}{\mathrm{d}\theta} \left(\mathcal{C}_{\mathrm{O}_2} \left(P_{\mathrm{O}_2}(\chi_{\mathrm{O}_2}(x,t),\theta), P_{\mathrm{CO}_2}(\chi_{\mathrm{CO}_2}(x,t),\theta) \right) \right) & = D_{m,\mathrm{O}_2} \left(\chi_{\mathrm{O}_2}(x,t) P_{\mathrm{atm}} - P_{\mathrm{O}_2}(\chi_{\mathrm{O}_2}(x,t),\theta) \right), \\ V_c \frac{\mathrm{d}}{\mathrm{d}\theta} \left(\mathcal{C}_{\mathrm{CO}_2} \left(P_{\mathrm{O}_2}(\chi_{\mathrm{O}_2}(x,t),\theta), P_{\mathrm{CO}_2}(\chi_{\mathrm{CO}_2}(x,t),\theta) \right) \right) & = D_{m,\mathrm{CO}_2} \left(\chi_{\mathrm{CO}_2}(x,t) P_{\mathrm{atm}} - P_{\mathrm{CO}_2}(\chi_{\mathrm{CO}_2}(x,t),\theta) \right), \end{cases}$$

where $\mathcal{C}_{\text{gas}}$ is the concentration of the considered gas in the blood, P_{gas} is the partial pressure of the gas in the blood during a cycle $[0, \tau_b]$, $D_{m,\text{gas}}$ is the diffusive capacity of the gas through the alveolar membrane, and P_{atm} is the atmospheric pressure. The dynamics of the gas concentration is then driven by the difference between partial pressures in the alveoli and in the blood. Note that (9) is solved at each time t and at each point x. Moreover note that the gas concentrations $\mathcal{C}_{\text{gas}}$ depend on the blood partial pressures of each species and the specific forms of these functions model the Bohr-Haldane effect. Here we consider the functions used in [7]. We complete this dynamical system with the following initial conditions at $\theta = 0$,

$$P_{\mathrm{O}_2}(\chi_{\mathrm{O}_2}(x,t),0) = \mathrm{P}_{v,\mathrm{O}_2}, \qquad P_{\mathrm{CO}_2}(\chi_{\mathrm{CO}_2}(x,t),0) = \mathrm{P}_{v,\mathrm{CO}_2},$$

where $\mathrm{P}_{v,\text{gas}}$ corresponds to the deoxygenated blood partial pressure of the considered gas, corresponding to blood which is poor in oxygen and rich in carbon dioxide, and is here considered as a constant value along the tree, namely in a healthy case at rest $\mathrm{P}_{v,\mathrm{O}_2} = 40$ mmHg, and $\mathrm{P}_{v,\mathrm{CO}_2} = 45$ mmHg [16].

Finally, we define the oxygen $\dot{V}_{\mathrm{O}_2}$ and carbon dioxide $\dot{V}_{\mathrm{CO}_2}$ fluxes that flow to and from the bloodstream. They are obtained by computing the difference between the concentration of the gas in the blood at time τ_b (oxygenated blood) and the concentration of the gas in the blood at the initial time (deoxygenated blood). They are written as

(10)
$$\begin{cases} \dot{V}_{\mathrm{O}_2}(\chi_{\mathrm{O}_2}(x,t), \chi_{\mathrm{CO}_2}(x,t)) & = \frac{V_c}{\tau_b} \left(\mathcal{C}_{\mathrm{O}_2} \left(P_{\mathrm{O}_2}(\chi_{\mathrm{O}_2}(x,t),\tau_b), P_{\mathrm{CO}_2}(\chi_{\mathrm{CO}_2}(x,t),\tau_b) \right) - \mathcal{C}_{\mathrm{O}_2} \left(\mathrm{P}_{v,\mathrm{O}_2}, \mathrm{P}_{v,\mathrm{CO}_2} \right) \right), \\ \dot{V}_{\mathrm{CO}_2}(\chi_{\mathrm{CO}_2}(x,t), \chi_{\mathrm{O}_2}(x,t)) & = \frac{V_c}{\tau_b} \left(\mathcal{C}_{\mathrm{CO}_2} \left(P_{\mathrm{O}_2}(\chi_{\mathrm{O}_2}(x,t),\tau_b), P_{\mathrm{CO}_2}(\chi_{\mathrm{CO}_2}(x,t),\tau_b) \right) - \mathcal{C}_{\mathrm{CO}_2} \left(\mathrm{P}_{v,\mathrm{O}_2}, \mathrm{P}_{v,\mathrm{CO}_2} \right) \right). \end{cases}$$

Let us mention that the partial pressure of the gas $\mathrm{P}_{a,\text{gas}}$ at each time t in the oxygenated blood is defined as the partial pressure of the gas obtained at the final time τ_b and is written as

$$\mathrm{P}_{a,\text{gas}}(t,x) = P_{\text{gas}}(\chi_{\text{gas}}(t,x), \tau_b).$$

In what follows, the arterial partial blood pressure shall denote the blood partial pressure in oxygenated blood.

2.5. **Full 1D coupled model.** Let us rewrite the whole model

$$
\begin{cases}
\textbf{Mechanical model} \\
-P(t) = E(V(t) - V_{\mathrm{FRC}}) + R\dot{V}(t), \\
\textbf{Conservation of air volume along the tree} \\
\partial_t \tilde{V} + \partial_x(Su) = 0, \quad \text{in } (0,L), \\
\textbf{Gas transport in the lung} \\
\partial_t(\tilde{V}\chi_{\mathrm{gas}}) + \partial_x(Su\chi_{\mathrm{gas}}) - D_{\mathrm{gas}}\partial_x(S\partial_x\chi_{\mathrm{gas}}) = -\frac{\tilde{\Sigma}}{\Sigma}\dot{V}_{\mathrm{gas}}, \quad \text{in } (0,L), \\
\textbf{Instantaneous gas fluxes through the alveolar membrane} \\
\dot{V}_{\mathrm{O_2}}(t,x) = \frac{V_c}{\tau_b}\left(\mathcal{C}_{\mathrm{O_2}}\left(P_{\mathrm{O_2}}(\chi_{\mathrm{O_2}}(t,x),\tau_b), P_{\mathrm{CO_2}}(\chi_{\mathrm{CO_2}}(t,x),\tau_b)\right) - \mathcal{C}_{\mathrm{O_2}}\left(\mathrm{P}_{v,\mathrm{O_2}}, \mathrm{P}_{v,\mathrm{CO_2}}\right)\right), \\
\dot{V}_{\mathrm{CO_2}}(t,x) = \frac{V_c}{\tau_b}\left(\mathcal{C}_{\mathrm{CO_2}}\left(P_{\mathrm{O_2}}(\chi_{\mathrm{O_2}}(t,x),\tau_b), P_{\mathrm{CO_2}}(\chi_{\mathrm{CO_2}}(t,x),\tau_b)\right) - \mathcal{C}_{\mathrm{CO_2}}\left(\mathrm{P}_{v,\mathrm{O_2}}, \mathrm{P}_{v,\mathrm{CO_2}}\right)\right), \\
\textbf{Instantaneous partial pressures in arterial blood at each time } t \textbf{ and } x \in [0,L] \\
\text{for } \theta \in [0,\tau_b], \\
\begin{cases}
V_c\frac{\mathrm{d}}{\mathrm{d}\theta}\left(\mathcal{C}_{\mathrm{O_2}}\left(P_{\mathrm{O_2}}(\chi_{\mathrm{O_2}}(t,x),\theta), P_{\mathrm{CO_2}}(\chi_{\mathrm{CO_2}}(t,x),\theta)\right)\right) &=& D_{m,\mathrm{O_2}}\left(\chi_{\mathrm{O_2}}(t,x)P_{\mathrm{atm}} - P_{\mathrm{O_2}}(\chi_{\mathrm{O_2}},\theta)\right), \\
V_c\frac{\mathrm{d}}{\mathrm{d}\theta}\left(\mathcal{C}_{\mathrm{CO_2}}\left(P_{\mathrm{O_2}}(\chi_{\mathrm{O_2}},\theta), P_{\mathrm{CO_2}}(\chi_{\mathrm{CO_2}}(t,x),\theta)\right)\right) &=& D_{m,\mathrm{CO_2}}\left(\chi_{\mathrm{CO_2}}(t,x)P_{\mathrm{atm}} - P_{\mathrm{CO_2}}(\chi_{\mathrm{CO_2}}(t,x),\theta)\right), \\
P_{\mathrm{O_2}}(\chi_{\mathrm{O_2}},0) = \mathrm{P}_{v,\mathrm{O_2}}, \qquad P_{\mathrm{CO_2}}(\chi_{\mathrm{CO_2}},0) = \mathrm{P}_{v,\mathrm{CO_2}}.
\end{cases}
\end{cases}
$$

Since one of our aims is to understand the time delay induced by the transport of air along the respiratory tree, we shall compare numerically the considered model to its 0D counterpart introduced and studied in [7], which we recall below for the sake of completeness.

2.6. **A 0D Model.** The 0D counterpart of our 1D model can be described as follows: we consider the same 0D mechanical model that provides the evolution of the lung volume $t \mapsto V(t)$. We assume that this volume is occupied by air, including a specific gas (e.g. O_2 and CO_2) with uniform molar fraction $t \mapsto \chi_{\mathrm{gas}}(t)$. The available volume for gas exchange is the volume V to which we subtract the dead volume, denoted V_D. This "dead space" volume does not take part in the exchange process and can be split in a physiological part and an anatomic part. The volume V_D is defined as the sum of a reference dead space and $\max(0, V_{\mathrm{endexpi}} - V_{\mathrm{FRC}})$, where V_{endexpi} denotes the end expiration volume at each breathing cycle. Since we are considering herein non-pathological situations, the dead volume should be close to the reference anatomical dead volume. Taking into account this dead space volume, it means that the volume of the specific gas in the lung volume is $\chi_{\mathrm{gas}}(V - V_D)$. During inspiration, the rate of gas which enters the balloon is $\overline{\chi}_{\mathrm{gas}}\dot{V} > 0$, which corresponds to a mixture of fresh air and lung air. Consequently $\overline{\chi}_{\mathrm{gas}}$ is defined by $\overline{\chi}_{\mathrm{gas}} = (1 - \phi(t))\chi^{\mathrm{atm}}_{\mathrm{gas}} + \phi(t)\chi_{\mathrm{gas}}$, with $\phi(t) = V_D/(V(t) - V_{\mathrm{endexpi}} + V_D)$, with $\chi^{\mathrm{atm}}_{\mathrm{O_2}} = 0.21$ and $\chi^{\mathrm{atm}}_{\mathrm{CO_2}} = 0.04$. During expiration, the rate of gas writes $\chi_{\mathrm{gas}}\dot{V} < 0$ as air is expelled (including gas at current fraction χ_{gas}). Now denoting by $\dot{V}_{\mathrm{gas}}$ the flux of gas which diffuses through the alveolar-blood membrane, the dynamics of the gas fraction in the lung is governed by

$$
\frac{\mathrm{d}}{\mathrm{d}t}\left(\chi_{\mathrm{gas}}(V - V_D)\right) = H(\dot{V})\overline{\chi}_{\mathrm{gas}}\dot{V} + (1 - H(\dot{V}))\chi_{\mathrm{gas}}\dot{V} - \dot{V}_{\mathrm{gas}},
$$

where $H(\cdot)$ is the Heaviside graph (characteristic function of $\mathbb{R}^+$). One obtains

$$\dot{\chi}_{\rm gas} = \frac{1}{V - V_D}\left(\dot{V}(1-\phi)(\chi_{\rm gas}^{\rm atm} - \chi_{\rm gas})H(\dot{V}) - \dot{V}_{\rm gas}\right).$$

The flux of oxygen $\dot{V}_{\rm O_2}$ and carbon dioxide $\dot{V}_{\rm CO_2}$ are defined as in the 1D model by (10) and the full reduced 0D model thus reads:

$$\begin{cases}
\textbf{Mechanical model} \\
-P(t) = E(V(t) - V_{\rm FRC}) + R\dot{V}(t), \\
\textbf{Gas exchange} \\
\dot{\chi}_{\rm gas}(t) = \frac{1}{V(t)-V_D}\left(\dot{V}(t)(1-\phi(t))(\chi_{\rm gas}^{\rm atm} - \chi_{\rm gas}(t))H(\dot{V}(t)) - \dot{V}_{\rm gas}(t)\right), \\
\textbf{Instantaneous gas fluxes through the alveolar membrane,} \\
\dot{V}_{\rm O_2}(t) = \dot{V}_{\rm O_2}(\chi_{\rm O_2}(t), \chi_{\rm CO_2}(t)) = \frac{V_c}{\tau_b}\left(\mathcal{C}_{\rm O_2}\left(P_{\rm O_2}(\chi_{\rm O_2}(t), \tau_b), P_{\rm CO_2}(\chi_{\rm CO_2}(t), \tau_b)\right) - \mathcal{C}_{\rm O_2}\left(\mathrm{P}_{v,\rm O_2}, \mathrm{P}_{v,\rm CO_2}\right)\right), \\
\dot{V}_{\rm CO_2}(t) = \dot{V}_{\rm CO_2}(\chi_{\rm CO_2}(t), \chi_{\rm O_2}(t)) = \frac{V_c}{\tau_b}\left(\mathcal{C}_{\rm CO_2}\left(P_{\rm CO_2}(\chi_{\rm CO_2}(t), \tau_b), P_{\rm O_2}(\chi_{\rm O_2}(t), \tau_b)\right) - \mathcal{C}_{\rm CO_2}\left(\mathrm{P}_{v,\rm CO_2}, \mathrm{P}_{v,\rm O_2}\right)\right), \\
\textbf{Instantaneous partial pressures in arterial blood at time } t, \theta \in [0, \tau_b], \\
\begin{cases}
V_c \frac{\rm d}{{\rm d}\theta}\left(\mathcal{C}_{\rm O_2}\left(P_{\rm O_2}(\chi_{\rm O_2}(t), \theta), P_{\rm CO_2}(\chi_{\rm CO_2}(t), \theta)\right)\right) &=& D_{m,\rm O_2}\left(\chi_{\rm O_2}(t)P_{\rm atm} - P_{\rm O_2}(\chi_{\rm O_2}(t), \theta)\right), \\
V_c \frac{\rm d}{{\rm d}\theta}\left(\mathcal{C}_{\rm CO_2}\left(P_{\rm O_2}(\chi_{\rm O_2}(t), \theta), P_{\rm CO_2}(\chi_{\rm CO_2}(t), \theta)\right)\right) &=& D_{m,\rm CO_2}\left(\chi_{\rm CO_2}(t)P_{\rm atm} - P_{\rm CO_2}(\chi_{\rm CO_2}(t), \theta)\right), , \\
P_{\rm O_2}(\chi_{\rm O_2}(t), 0) = \mathrm{P}_{v,\rm O_2}, \qquad P_{\rm CO_2}(\chi_{\rm CO_2}(t), 0) = \mathrm{P}_{v,\rm CO_2}.
\end{cases}
\end{cases}$$

Note that in this 0D model, the mixing of fresh air and lung air as well as the dead space have to be taken into account to recover standard physiological behavior (see Remark 8 in [7]). In the 1D model, this mixing and the dead space are taken into account by the "geometry". Indeed, the mixing takes place during air transport along the bronchial tree, in which there is no gas exchange, and this bronchial region represents the dead space region.

2.7. **Inputs of the models.** Let us note that our model is totally controlled by the pleural pressure $t \mapsto P(t)$. This function is the driving force of ventilation. It is regulated to achieve good gas exchanges. Our aim is to explore numerically the ability of our 1D model to reproduce normal breathing scenarios. We shall consider periodic breathing scenarios with two different shapes: in the first scenario, the applied pressure on the lung is piecewise constant and is given by

$$P(t) = \begin{cases} \mathrm{P}_{\rm insp}, & t \in [0, {\rm IE} \times T[\,, \\ \mathrm{P}_{\rm exp}, & t \in [{\rm IE} \times T, T[\,, \end{cases} \tag{11}$$

where T is the respiratory cycle period and IE is the inspiratory ratio. Typical values for normal breathing are given by

$$T = 5\,{\rm s}, \quad {\rm IE} = 0.4, \quad \mathrm{P}_{\rm insp} = -2\,{\rm cmH_2O}, \quad \mathrm{P}_{\rm exp} = 0\,{\rm cmH_2O}.$$

In the second scenario, we propose another pressure pattern: we consider an increasing (resp. decreasing) exponential shape at inspiration (resp. expiration). This scenario corresponds to a piecewise constant muscle activity. This signal is transformed into an exponential applied pressure through a resistance-compliance (R_mC) model, also called the Voigt model of viscoelastic behavior [28]. It is given by

$$P_m(t) = \tau \dot{P}(t) + P(t), \tag{12}$$

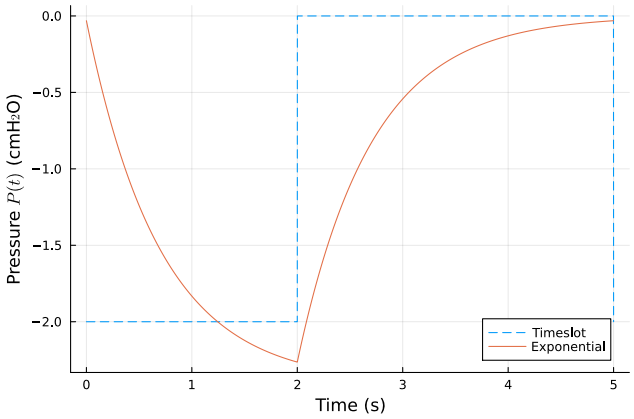

FIGURE 3. Pleural pressure for two scenarios: Timeslot profile defined by (11) with $T = 5$ s, $\mathrm{P}_{\mathrm{insp}} = -2.0$ cmH$_2$O, $\mathrm{P}_{\mathrm{exp}} = 0$ cmH$_2$O, IE $= 0.4$, vs. Exponential profile defined by (12) with $T = 5$ s, $\mathrm{P}_{\mathrm{insp}} = -2.4$ cmH$_2$O, $\mathrm{P}_{\mathrm{exp}} = 0$ cmH$_2$O, IE $= 0.4$. Both scenarios correspond to the same tidal volume $V_T = 0.49$ L.

where $P_m(t)$ is the muscle activity pressure, $\tau = R_m C$ is the characteristic time and $P(t)$ is the pressure applied on the lung. The pressure applied on the respiratory muscles is defined as follows:

$$P_m(t) = \begin{cases} \mathrm{P}_{\mathrm{insp}}, & t \in [0, \mathrm{IE} \times T[\,, \\ \mathrm{P}_{\mathrm{exp}}, & t \in [\mathrm{IE} \times T, T[\,. \end{cases} \tag{13}$$

The reference exponential pattern has been chosen with characteristic time $\tau = 0.7$ s and typical values for normal breathing are given by

$$T = 5\,\mathrm{s}, \quad \mathrm{IE} = 0.4, \quad \mathrm{P}_{\mathrm{insp}} = -2.4\,\mathrm{cmH_2O}, \quad \mathrm{P}_{\mathrm{exp}} = 0\,\mathrm{cmH_2O}.$$

This breathing scenario leads to a tidal volume of 0.49 L, as obtained with the piecewise constant pattern. Standard breathing patterns are illustrated in Fig. 3.

Note that the time period of 5 s, the inspiratory time of 2 s (corresponding thus to IE $= 0.4$), passive expiration (corresponding thus to $\mathrm{P}_{\mathrm{exp}} = 0$), and an inspiratory pressure around 2.5 mmHg (see [16]) are the parameters observed in practice that we would like to recover from our optimal study.

2.8. **Outputs of the models and cost functions.** For comparison purposes and sensitivity analysis, we choose to consider the following outputs of our models:

- The mean amount of oxygen and carbon dioxide exchanged with the blood during a respiratory cycle. It is computed thanks to the following expression

$$\overline{\dot{V}}_{\mathrm{gas}} = \frac{1}{T} \int_0^T \left(\int_0^L \frac{\tilde{\Sigma}(x)}{\Sigma} \dot{V}_{\mathrm{gas}}(t,x) \mathrm{d}x \right) \mathrm{d}t. \tag{14}$$

- The mean arterial partial pressure of oxygen and carbon dioxide during a respiratory cycle. It is written as

$$\overline{\mathrm{P}}_{a,\mathrm{gas}} = \frac{1}{T} \int_0^T \left(\int_0^L \frac{\tilde{\Sigma}(x)}{\Sigma} \mathrm{P}_{a,\mathrm{gas}}(t,x) \mathrm{d}x \right) \mathrm{d}t. \tag{15}$$

- The tidal volume V_T, which is the amount of air inhaled during a respiratory cycle.

- The respiratory quotient, defined by

$$\mathrm{RQ} = \frac{-\overline{\dot{V}}_{\mathrm{CO_2}}}{\overline{\dot{V}}_{\mathrm{O_2}}}.$$

For a normal breathing scenario and in the healthy case, the standard values are [16, 22, 49]:

$$V_T = 0.5\,\mathrm{L},\ \overline{\dot{V}}_{\mathrm{O_2}} = 250\,\mathrm{mL}\cdot\mathrm{min}^{-1},\ \overline{\dot{V}}_{\mathrm{CO_2}} = -200\,\mathrm{mL}\cdot\mathrm{min}^{-1},\ \mathrm{RQ} = 0.8,$$

$$\overline{\mathrm{P}}_{a,\mathrm{O_2}} = 100\,\mathrm{mmHg},\ \overline{\mathrm{P}}_{a,\mathrm{CO_2}} = 40\,\mathrm{mmHg}.$$

We shall also consider the following components of the cost function to select the optimal scenario:

- The power of external forces $\mathcal{W}$, which is defined as the opposite of the product between the applied pleural pressure and the airflow going through the lung [26] and is written

$$\mathcal{W} = \frac{1}{T}\int_0^T -P(t)\dot{V}(t)\,\mathrm{d}t. \tag{16}$$

  Thanks to equation (5), and to the fact that $V(T) = V(0)$ we can rewrite it as

$$\mathcal{W} = \frac{1}{T}\int_0^T R\dot{V}^2(t)\,\mathrm{d}t \geqslant 0.$$

- The variation of the maximal volume with respect to a given V_{FRC} which corresponds to the amount of distension of the lung during a respiratory cycle and is written

$$\mathcal{D}_V = (V_{\max} - V_{\mathrm{FRC}})^2.$$

Moreover, we recall that the respiratory cycle adapts to maintain an arterial pressure of carbon dioxide around 40 mmHg.

2.9. **Numerical methods.** We use the same numerical method as in [24]. First, we discretize the mechanical 0D model (5) using an implicit Euler scheme. It gives us the volume V and the flux $\dot{V}$ which corresponds also to to the time derivative of the volume at each time.

Next, our PDEs are approximated using a finite volume scheme. We discretize the time interval $[0, T]$ with N points $(t^n)_{1\leq i\leq N}$ and the space domain $[0, L]$ with M points $(x^i)_{1\leq i\leq M}$. Let us define at each nodes $(x^i, t^n)_{i=1,\dots,M}^{n=1\dots N}$, the derivative of the lineic volume $\partial_t\tilde{V}^{i,n}$ which corresponds to the airflow $\dot{V}^{i,n}$ per unit of length. The conservation of air volume can then be discretized with an upwind scheme, which reads

$$\left(\frac{(Su)^{i,n} - (Su)^{i-1,n}}{\Delta x_g}\right)\mathbb{1}_{\dot{V}^n>0} + \left(\frac{(Su)^{i+1,n} - (Su)^{i,n}}{\Delta x_g}\right)\mathbb{1}_{\dot{V}^n\leqslant 0} = -\partial_t\tilde{V}^{i,n}, \tag{17}$$

where Δx_g is an adaptive space step depending on the gth generation. Since the length of the bronchi decreases generation by generation, this adaptive space step is needed to have enough discretization points in the last generations of the respiratory tree without refining the whole domain. We choose Δx_g such that we have the same number of points per generation. We complete our equation with the following boundary conditions: $(Su)^{1,n} = \dot{V}^n$ during inspiration ($\dot{V}^n > 0$) and $(Su)^{M,n} = 0$ at expiration ($\dot{V}^n < 0$).

Let us now denote $\chi_{\mathrm{gas}}^{i,n}$ the approximations of the mole fractions at each point (x^i, t^n). The transport equation of the respiratory gases is then discretized as

$$\frac{\left(\tilde{V}\chi_{\mathrm{gas}}\right)^{i,n+1} - \left(\tilde{V}\chi_{\mathrm{gas}}\right)^{i,n}}{\Delta t} + \frac{\left(\Phi_{\mathrm{gas}}^{i+1/2,n+1} - \Phi_{\mathrm{gas}}^{i-1/2,n+1}\right)}{\Delta x_g} = -\frac{\tilde{\Sigma}(x^i)}{\Sigma}\dot{V}_{\mathrm{gas}}^{i,n}, \tag{18}$$

where $\Phi_{\text{gas}}^{i+1/2,n+1}$ and $\Phi_{\text{gas}}^{i-1/2,n+1}$ are approximations of the total flux which can be expressed as

$$\begin{cases} \Phi_{\text{gas}}^{i+1/2,n+1} = (Su)^{i,n+1}\chi_{\text{gas}}^{i,n+1}\mathbb{1}_{\dot{V}^n>0} + (Su)^{i+1,n+1}\chi_{\text{gas}}^{i+1,n+1}\mathbb{1}_{\dot{V}^n\leqslant 0} - D_{\text{gas}}S^{i+1/2,n+1}\frac{\chi_{\text{gas}}^{i+1,n+1}-\chi_{\text{gas}}^{i,n+1}}{\Delta x_g}, \\ \Phi_{\text{gas}}^{i-1/2,n+1} = (Su)^{i-1,n+1}\chi_{\text{gas}}^{i-1,n+1}\mathbb{1}_{\dot{V}^n>0} + (Su)^{i,n+1}\chi_{\text{gas}}^{i,n+1}\mathbb{1}_{\dot{V}^n\leqslant 0} - D_{\text{gas}}S^{i-1/2,n+1}\frac{\chi_{\text{gas}}^{i,n+1}-\chi_{\text{gas}}^{i-1,n+1}}{\Delta x_g}. \end{cases}$$

We complete the equations with boundary conditions that depend on the breathing cycle. During inspiration, we assume that the molar fraction at the entrance of the trachea is the same as the one in the air, $\chi_{\text{gas}}^{1,n} = \chi_{\text{gas}}^{\text{atm}}$, and during expiration, we assume that there is a free flux at the entrance of the trachea, $\chi_{\text{gas}}^{1,n} = \chi_{\text{gas}}^{2,n}$. For the whole breathing cycle, we impose at the tree terminals that $\Phi_{\text{gas}}^{M+1/2,n} = 0$.

Note that the flux $\dot{V}_{\text{gas}}^{i,n}$ is treated in an explicit way in (18) and computed from the previous time step. More precisely, the approximation of the oxygen and carbon dioxide fluxes $\dot{V}_{\text{gas}}$ are computed by resolving the differential equations (9) using a 4th order Runge-Kutta scheme. Thanks to this resolution, we have access to the approximation of the arterial partial pressure of the each gas at each node $\mathrm{P}_{a,\text{gas}}^{n,i} = P_{\text{gas}}(\chi_{\text{gas}}^{i,n}, \tau_b)$. We can then compute the mean value of the partial pressure of the gases in the arterial blood during a respiratory cycle with

$$\overline{\mathrm{P}}_{a,\text{gas}} = \frac{1}{N}\sum_{n=1}^{N}\sum_{i=1}^{M}\frac{\tilde{\Sigma}(x^i)}{\Sigma}\Delta x_g \mathrm{P}_{a,\text{gas}}^{n,i}, \tag{19}$$

where $\tilde{\Sigma}$ corresponds to the lineic alveolar surface defined previously in equation (3) and Σ corresponds to the total alveolar surface.

Likewise, we can compute the mean amount of oxygen and carbon dioxide exchanged with the blood during a respiratory cycle by

$$\overline{\dot{V}}_{\text{gas}} = \frac{1}{N}\sum_{n=1}^{N}\sum_{i=1}^{M}\frac{\tilde{\Sigma}(x^i)}{\Sigma}\Delta x_g \dot{V}_{\text{gas}}^{i,n}. \tag{20}$$

3. Results

In this section, we numerically investigate the behavior of the two models. First we consider the 1D model only, for standard breathing scenario in the healthy case and perform a sensitivity analysis with respect to the model parameters. We also explore breathing during exercise and provide carbon dioxide washout curves. Then we compare the 0D model and 1D model by performing simulations with different applied pressures, varying T, IE and P_{insp}, while P_{exp} remains constant and equal to 0 $\mathrm{cmH_2O}$. This choice is motivated by the fact that in normal breathing, exhalation is passive and thus, no muscular effort is exerted by the diaphragm muscle [16, 22]. The objectives are multiple:

- to evaluate the ability of the 1D model to recover standard physiological behavior in normal breathing conditions (at rest and during exercise);
- to investigate the importance of the time delay induced by gas transport along the tree;
- to assess the sensitivity of the models with respect to the applied pressure;
- to analyze the criteria that the normal breathing scenario may optimize;
- to understand the ability of each model to faithfully reproduce physiological behavior.

Note that to ensure convergence toward the periodic solution for each simulation, we perform multiple respiratory cycles (typically around 100).

In all the simulations (except during exercise or for the sensitivity analysis of parameters), we use the same physiological parameters, which correspond to standard values reported in the literature for normal breathing in healthy conditions (see Section A and Table 14). Moreover, the geometric parameters correspond to physiological values provided by [48].

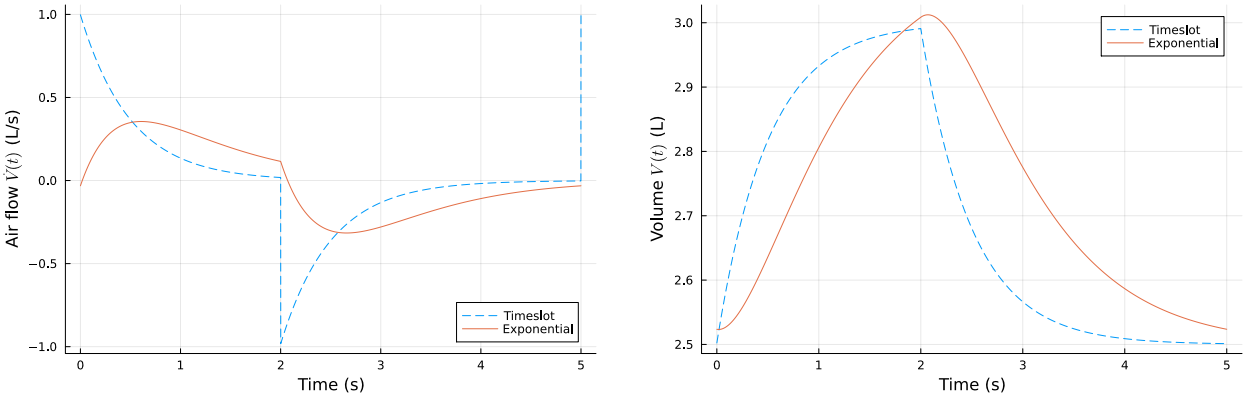

FIGURE 4. Airflow $t \mapsto \dot{V}(t)$ and lung volume $t \mapsto V(t)$ for two scenarios of pleural pressure: Timeslot profile defined by (11) with $T = 5$ s, $\mathrm{P}_{\mathrm{insp}} = -2.0$ $\mathrm{cmH_2O}$, $\mathrm{P}_{\mathrm{exp}} = 0$ $\mathrm{cmH_2O}$, IE $= 0.4$ vs. Exponential profile defined by (12) with $T = 5$ s, $\mathrm{P}_{\mathrm{insp}} = -2.4$ $\mathrm{cmH_2O}$, $\mathrm{P}_{\mathrm{exp}} = 0$ $\mathrm{cmH_2O}$, IE $= 0.4$. Each scenario corresponds to the same tidal volume $V_T = 0.49$ L.

3.1. **1D model.** Let us first present numerical simulations of the 1D model for two different external forcing terms corresponding to Fig. 3. The associated periodic volume and flux are given by Fig. 4. In particular, the airflow instantaneously reaches its peak at the beginning of inhalation and exhalation for the timeslot pattern, while the airflow dynamics are smoother for the exponential pressure pattern. Nevertheless, both scenarios correspond to a similar maximal inhaled volume and a similar tidal volume V_T. Note that in the exponential case, the lung volume does not return exactly to V_{FRC}, and the airflow profile remains smoother throughout the cycle. Despite these differences, the average values over one period, per generation, are strongly similar (see Fig. 5) as are the average fluxes over time. We also observe that the gas exchange fluxes are particularly significant at the tree terminals.

In Fig. 6, the magnitudes and time evolution of the average oxygen and carbon dioxide fluxes are very similar in both scenarios and a time delay can be observed in both cases: shorter in the timeslot case and surely due to the transport along the tree. A larger time delay coming from the exponential pattern of the pressure appears in the other case. The same time delay is observed in Fig. 7 for the time evolution of the alveolar partial pressure of oxygen and carbon dioxide in different regions of the bronchial tree. Observe that, at the end of the acinus, the partial pressures of oxygen and carbon dioxide are almost constant over time and equal to 100 mmHg for oxygen and 40 mmHg for carbon dioxide, which are the values in the oxygenated blood partial pressure [16, 22, 49].

Furthermore, the main gas exchanges take place in the last generations of the tree and in particular 73% of the exchanges take place in the last two generations. Moreover, we see that the standard mean outputs values defined in Section 2.8 are recovered for both breathing scenarios in Table 1, without any fitting of the model parameters.

3.1.1. *Sensitivity analysis with respect to the physiological parameters.* In this subsection, we investigate the sensitivity of the 1D model with respect to the physiological parameters. We consider a healthy case and look at the different outputs while varying the parameters given in Table 14. To do so, we quantify the dependence of the mean fluxes and partial pressures $(\overline{\dot{V}}_{\mathrm{O_2}}, \overline{\dot{V}}_{\mathrm{CO_2}}, \overline{\mathrm{P}}_{a,\mathrm{O_2}}, \overline{\mathrm{P}}_{a,\mathrm{CO_2}})$ with respect to the physiological parameters by computing the following dimensionless sensitivity

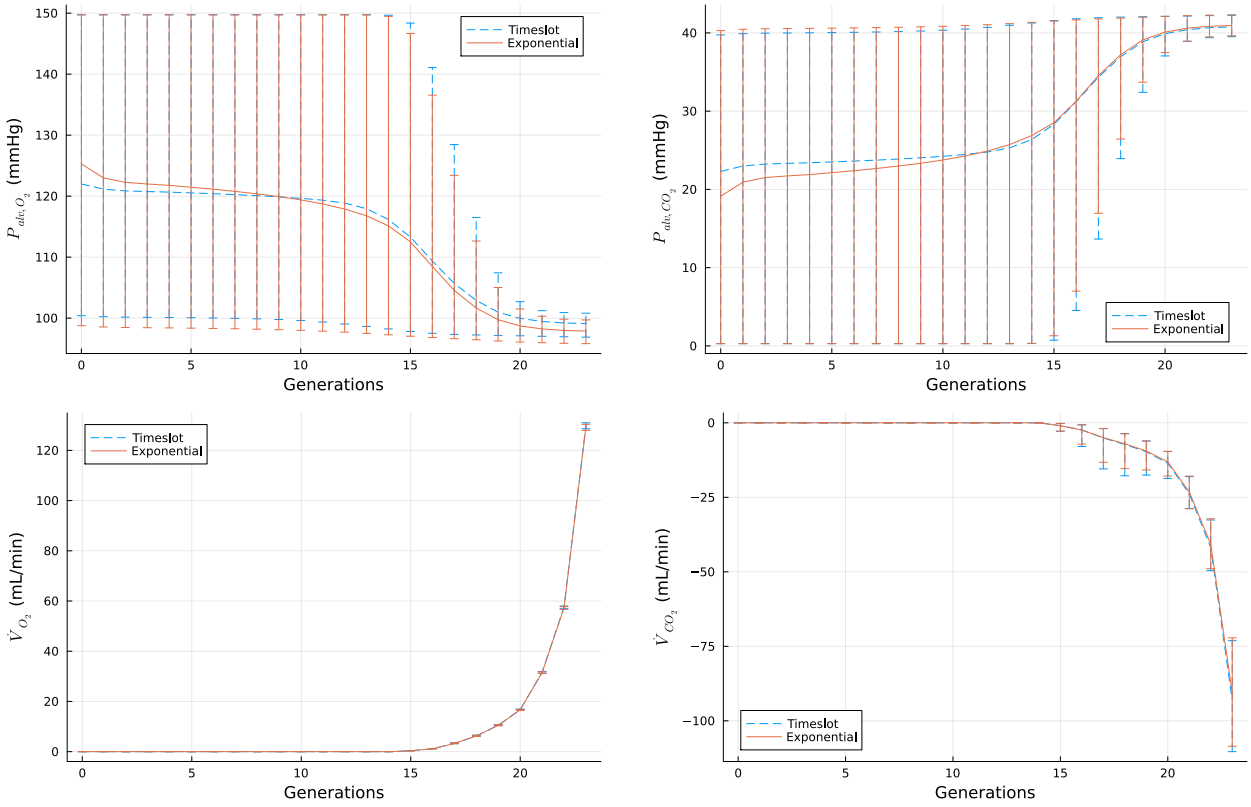

FIGURE 5. Time average by generation of $\mathrm{P_{alv,O_2}}$, $\mathrm{P_{alv,CO_2}}$, $\dot{V}_{\mathrm{O_2}}$, $\dot{V}_{\mathrm{CO_2}}$ for both scenarios: piecewise constant applied pressure defined by (11) with $T = 5$ s, $\mathrm{P_{insp}} = -2$ $\mathrm{cmH_2O}$, $\mathrm{P_{exp}} = 0$ $\mathrm{cmH_2O}$, IE $= 0.4$ and piecewise exponential defined by (12) with $T = 5$ s, $\mathrm{P_{insp}} = -2.4$ $\mathrm{cmH_2O}$, $\mathrm{P_{exp}} = 0$ $\mathrm{cmH_2O}$, IE $= 0.4$.

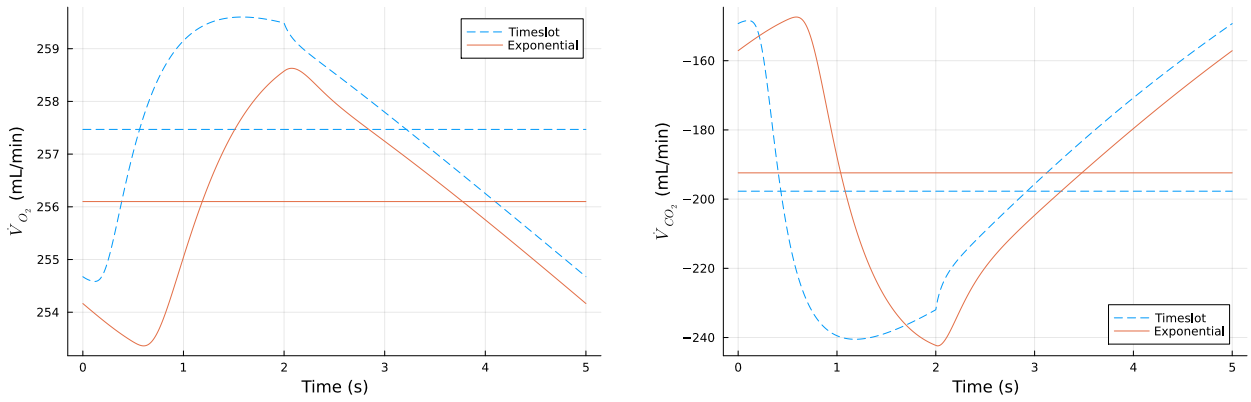

FIGURE 6. Time evolution of $\dot{V}_{\mathrm{O_2}}$, $\dot{V}_{\mathrm{CO_2}}$, for both scenarios: piecewise constant applied pressure, defined by (11) with $T = 5$ s, $\mathrm{P_{insp}} = -2$ $\mathrm{cmH_2O}$, $\mathrm{P_{exp}} = 0$ $\mathrm{cmH_2O}$, IE $= 0.4$ and piecewise exponential, defined by (12) with $T = 5$ s, $\mathrm{P_{insp}} = -2.4$ $\mathrm{cmH_2O}$, $\mathrm{P_{exp}} = 0$ $\mathrm{cmH_2O}$, IE $= 0.4$.

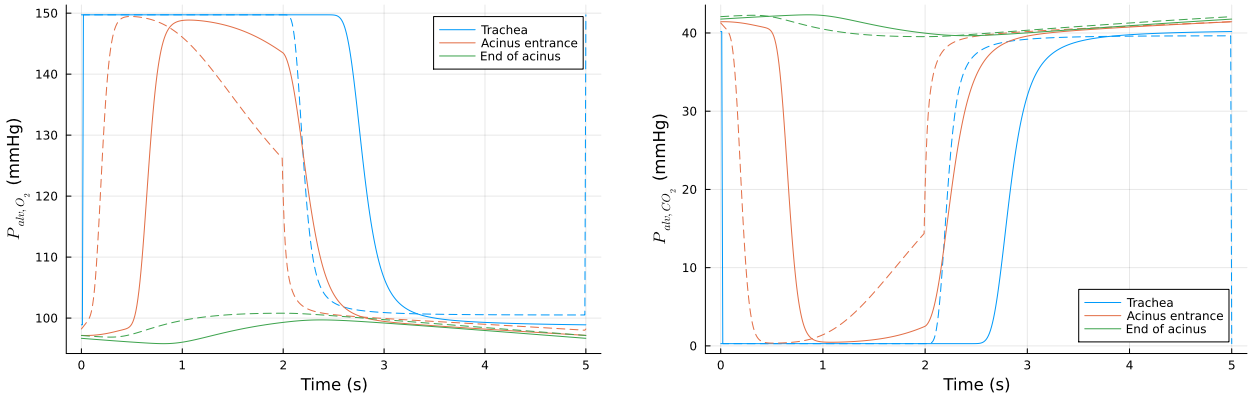

FIGURE 7. Time evolution of the alveolar pressure $\mathrm{P}_{\mathrm{alv,O_2}}$ (left) and $\mathrm{P}_{\mathrm{alv,CO_2}}$ (right) for both scenarios: piecewise constant applied pressure, defined by (11) with $T = 5$ s, $\mathrm{P}_{\mathrm{insp}} = -2$ cmH$_2$O, $\mathrm{P}_{\mathrm{exp}} = 0$ cmH$_2$O, IE $= 0.4$ (dot line) and piecewise exponential, defined by (12) with $T = 5$ s, $\mathrm{P}_{\mathrm{insp}} = -2.4$ cmH$_2$O, $\mathrm{P}_{\mathrm{exp}} = 0$ cmH$_2$O, IE $= 0.4$ (plain line).

1D model	Timeslot	Exponential
$\overline{\dot{V}}_{\mathrm{O_2}}$ (mL/min)	258	256
$\overline{\dot{V}}_{\mathrm{CO_2}}$ (mL/min)	-200	-192
RQ	0.78	0.75
$\overline{\mathrm{P}}_{a,\mathrm{O_2}}$ (mmHg)	100.1	98.3
$\overline{\mathrm{P}}_{a,\mathrm{CO_2}}$ (mmHg)	40.3	40.5
V_T (L)	0.49	0.49

TABLE 1. Mean outputs over a breathing cycle provided by the resolution of the 1D problem for both scenarios: piecewise constant applied pressure, defined by (11) with $T = 5$ s, $\mathrm{P}_{\mathrm{insp}} = -2$ cmH$_2$O, $\mathrm{P}_{\mathrm{exp}} = 0$ cmH$_2$O, IE $= 0.4$ and piecewise exponential, defined by (12) with $T = 5$ s, $\mathrm{P}_{\mathrm{insp}} = -2.4$ cmH$_2$O, $\mathrm{P}_{\mathrm{exp}} = 0$ cmH$_2$O, IE $= 0.4$.

coefficients:

$$S_\alpha(\beta) := \frac{\partial \beta}{\partial \alpha}\frac{\alpha}{\beta}, \tag{21}$$

where α is a physiological parameter and β is an output of the model. The sensitivity coefficients $S_\alpha(\beta)$ quantify the relative change in the output β when the parameter α varies. Table 2 presents the sensitivity coefficients for the different outputs of the model with respect to the considered physiological parameters. The values are computed for a healthy case with a piecewise constant applied pressure defined by equation (11) with $T = 5$ s, $\mathrm{P}_{\mathrm{insp}} = -2.0$ cmH$_2$O, $\mathrm{P}_{\mathrm{exp}} = 0$ cmH$_2$O and IE $= 0.4$. The same tendencies are observed for a piecewise exponential applied pressure.

We can observe, as in [24], that the sensitivity of the outputs to the membrane diffusing capacities is zero. This is due, in the healthy resting state, to the equilibrium of partial pressures that occurs in a time shorter than τ_b. As a result, the system is robust with respect to D_m in this situation, allowing D_m to be reduced without affecting the gas exchanges with the blood, as long as it is not reduced too much. Furthermore, the sensitivity coefficients show that the output variables are very sensitive to the capillary volume V_c and the transit time τ_b. In particular, the blood partial pressure of oxygen $\overline{\mathrm{P}}_{a,\mathrm{O_2}}$ is negatively correlated with V_c and positively correlated with τ_b, which is expected

Parameter	$\overline{\dot{V}}_{O_2}$	$\overline{\dot{V}}_{CO_2}$	$\overline{P}_{a,O_2}$	$\overline{P}_{a,CO_2}$
Capillary volume (V_c)	+0.81	+0.15	-0.40	+0.12
Transit time (τ_b)	-0.78	-0.15	+0.38	-0.15
Membrane diffusing capacity of O_2 (D_{m,O_2})	0.00	0.00	0.00	0.00
Membrane diffusing capacity of CO_2 (D_{m,CO_2})	0.00	0.00	0.00	0.00
Pressure of O_2 at 50% saturation (P_{50})	+1.32	+0.10	-0.66	+0.07
Elastance (E)	-0.23	-1.0	-0.51	+0.17
Resistance (R)	-0.04	-0.25	-0.11	0.02

TABLE 2. Sensitivity of the respiratory gases flow through the alveolo capillary membrane and of the respiratory gases arterial partial pressures with respect to physiological parameters.

since a larger capillary volume leads to a lower oxygen partial pressure in the blood, while a longer transit time allows for more oxygen to be absorbed.

We can also observe that there is a strong positive dependence of P_{50} (which is defined as the oxygen partial pressure that corresponds to a 50% saturation of hemoglobin) on the oxygen flux to the blood. Indeed, the gas flux is mainly defined as the difference in oxygen concentration between oxygenated and deoxygenated blood (see (10)), and these concentrations depend on the Hill oxygen saturation curve (see [24]). For an oxygen partial pressure around 100 mmHg (corresponding to oxygenated blood), the Hill curve does not depend on P_{50}. However, for an oxygen partial pressure around 40 mmHg (corresponding to deoxygenated blood), there is a strong variation in the Hill saturation curve when P_{50} varies, which implies a strong variation in the concentration of O_2 in the deoxygenated blood.

3.1.2. *Exercise.* In this subsection, we provide evidence of the ability of our 1D model to reproduce gas diffusion for breathing during exercise. Simulating moderate exercise with our 1D model consists in defining suitable parameters adapted to this regime: pulmonary capillary blood volume and diffusing membrane capacity increase secondary to a rise in pulmonary artery pressure and central blood volume mobilization. This can be done in our model by multiplying by 2 the capillary volume V_c [44] and the diffusion capacity [16, 44, 49], and by dividing by 3 the transit time τ_b [16]. Furthermore, the deoxygenated partial pressure of O_2 decreases by 10 mmHg [46], going from 40 mmHg to 30 mmHg and the deoxygenated partial pressure of CO_2 rises by 10 mmHg [8] which implies a change from 45 mmHg to 55 mmHg.

The breathing scenario also has to be changed with a lower period, namely $T = 2$ s, and a higher tidal volume to enable suitable gas exchanges, here we consider $V_T = 1.8$ L. The mean outputs of the model are summarized in Table 3. We can observe that the gas fluxes are multiplied by a factor 10 enabling the system to maintain suitable levels of oxygen and carbon dioxide blood partial pressures as observed in physiology [49].

We also recover from the gas fluxes along the bronchial tree (see Fig 8) that the gas exchanges with blood mainly take place in the last generations of the tree like in the resting case (see Fig 5).

3.1.3. CO_2 *washout curve.* In order to assess the robustness of our 1D model, we also choose to reproduce a CO_2 washout curve. This curve is obtained in clinical practice, by measuring at the mouth, the carbon dioxide concentration present in the air expelled from the lung with respect to the exhaled volume. This quantity is indeed an output of the 1D model since the spatial dimension is taken into account, contrary to the 0D model which computes only the concentration of the gases in the alveoli. An example of the CO_2 washout curve can be found in [40] and both piecewise constant and piecewise exponential scenarios allow us to recover the right shape and amplitude. Note that the exponential scenario leads to a shape and values that are closer to what is expected experimentally (see Fig. 1 p. 680 in [40]), in particular in the first and third phases of the curve.

1D model	Timeslot	Exponential
$\overline{\dot{V}}_{O_2}$ (L/min)	2.24	2.25
$\overline{\dot{V}}_{CO_2}$ (L/min)	-2.52	-2.54
RQ	1.13	1.13
$\overline{P}_{a,O_2}$ (mmHg)	107.5	107.9
$\overline{P}_{a,CO_2}$ (mmHg)	40.3	40.1
V_T (L)	1.80	1.80

TABLE 3. Mean outputs during exercise over a breathing cycle provided by the resolution of the 1D problem for both scenarios: piecewise constant applied pressure, defined by (11) with $T = 2$ s, $P_{insp} = -5.0$ cmH$_2$O, $P_{exp} = +4.5$ cmH$_2$O, IE $= 0.5$ and piecewise exponential, defined by (12) with $T = 2$ s, $P_{insp} = -12.4$ cmH$_2$O, $P_{exp} = +12$ cmH$_2$O, IE $= 0.5$.

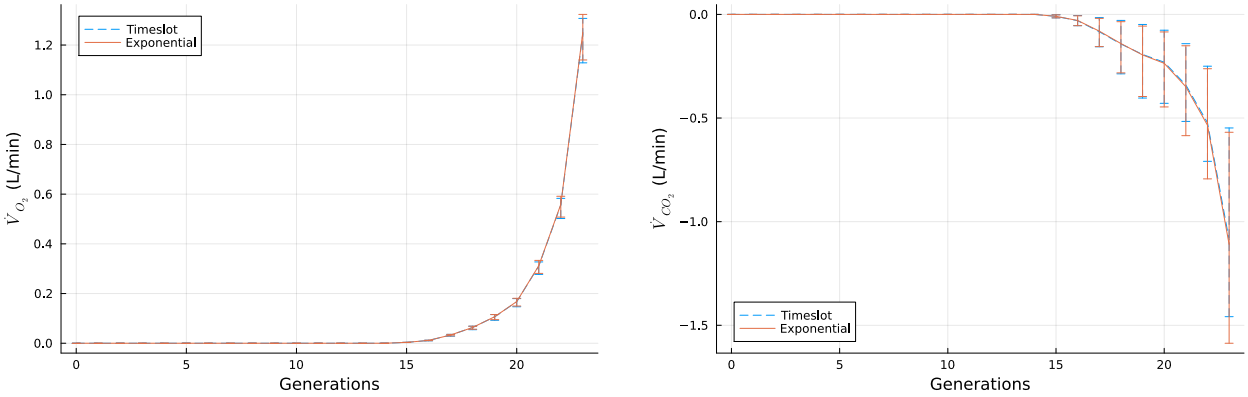

FIGURE 8. Time average by generation of $\dot{V}_{O_2}$ and $\dot{V}_{CO_2}$ for both scenarios: piecewise constant applied pressure defined by (11) with $T = 2$ s, $P_{insp} = -5$ cmH$_2$O, $P_{exp} = +4.5$ cmH$_2$O, IE $= 0.5$ and piecewise exponential defined by (12) with $T = 2$ s, $P_{insp} = -12.4$ cmH$_2$O, $P_{exp} = +12$ cmH$_2$O, IE $= 0.5$.

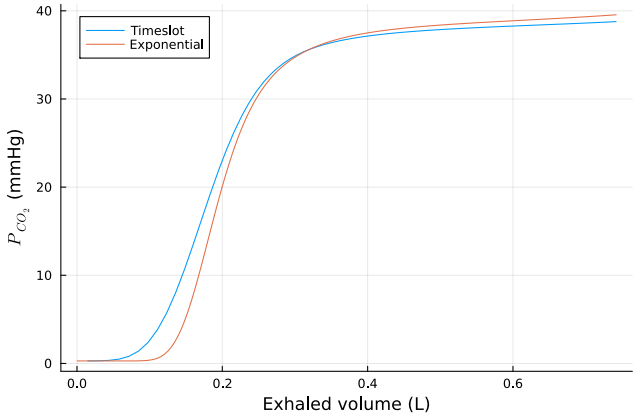

FIGURE 9. CO_2 washout curves for different breathing scenarios: in blue, the pressure applied on the lung is piecewise exponential, in red, the pressure applied on the lung is piecewise constant.

0D model	Timeslot	Exponential
$\overline{\dot{V}}_{O_2}$ (mL/min)	250	247
$\overline{\dot{V}}_{CO_2}$ (mL/min)	-179	-172
RQ	0.72	0.70
$\overline{P}_{a,O_2}$ (mmHg)	92.9	90.9
$\overline{P}_{a,CO_2}$ (mmHg)	40.9	41.1
V_T (L)	0.49	0.49

TABLE 4. Mean outputs over a breathing cycle provided by the resolution of the 0D problem for both scenarios: piecewise constant applied pressure, defined by (11) with $T = 5$ s, $P_{insp} = -2$ cmH$_2$O, $P_{exp} = 0$ cmH$_2$O, IE $= 0.4$ and piecewise exponential, defined by (12) with $T = 5$ s, $P_{insp} = -2.4$ cmH$_2$O, $P_{exp} = 0$ cmH$_2$O, IE $= 0.4$.

	0D Model	1D Model
$\overline{\dot{V}}_{O_2}$ (mL/min)	272	262
$\overline{\dot{V}}_{CO_2}$ (mL/min)	-286	-201
RQ	1.05	0.77
$\overline{P}_{a,O_2}$ (mmHg)	114.2	103.7
$\overline{P}_{a,CO_2}$ (mmHg)	37.3	40.3
V_T (L)	0.40	0.40

TABLE 5. 1D vs 0D models in hyperventilation: piecewise constant applied pressure defined by (11) with $T = 2$ s, $P_{insp} = -4.9$ cmH$_2$O, $P_{exp} = 0$ cmH$_2$O, IE $= 0.1$.

3.2. **Models comparison.** The 1D model has been developed in order to take into account the heterogeneity of transport and gas exchanges along the bronchial tree. The 1D structure has an impact on the gas exchange, due to the time that is required for fresh air to reach the acinus through the physiological dead space. However, it is expected that the 0D and 1D models provide similar results for average outputs, at least, in the healthy case under normal breathing conditions.

Indeed, for both considered scenarios, the two models behave in a really similar manner as stated by the results summarized in Table 1 for the 1D model and Table 4 for the 0D model.

As observed in Table 1 and Table 4, the main observable quantities of interest are only slightly affected by the choice of the pressure model in the normal regime with healthy parameters.

3.2.1. *Dependency of the 1D and 0D models with respect to the inspiratory fraction.* To further explore the effect of the transit time in the bronchial tree, let us consider breathing scenarios with different inspiratory ratios.

In order to investigate the differences between the two models, let us first consider three hyperventilation piecewise constant scenarios. A hyperventilation scenario is characterized by a breathing pattern such that the minute volume, defined by $60V_T/T$ is greater than the one in the reference case (which corresponds to a value of 6 L/min in the considered reference case). We consider only a piecewise constant breathing pattern in order to compare the models with no time delay in the applied pressure.

In Table 5, corresponding to a small period ($T = 2$ s), a large inspiratory pressure ($P_{insp} = -4.9$ cmH$_2$O), and a small inspiratory ratio (IE $= 0.1$), the output values for the 1D model are similar yet slightly higher than for the reference case (see Table 1), whereas for the 0D model the exchanges are improved compared to the reference case (see Table 4). Here, as the inspiratory ratio is small compared to the transit time in the bronchial tree, the exchanges cannot be improved for the 1D model as they are with the 0D model where the time delay is not taken into account.

	0D Model	1D Model
$\overline{\dot{V}}_{O_2}$ (mL/min)	264	274
$\overline{\dot{V}}_{CO_2}$ (mL/min)	-231	-295
RQ	0.87	1.08
$\overline{P}_{a,O_2}$ (mmHg)	104.6	118.1
$\overline{P}_{a,CO_2}$ (mmHg)	39.1	37.0
V_T (L)	0.40	0.40

TABLE 6. 1D vs 0D models in hyperventilation: : piecewise constant applied pressure defined by (11) with $T = 2$ s, $P_{insp} = -2.0$ cmH$_2$O, $P_{exp} = 0$ cmH$_2$O, IE $= 0.7$.

	0D Model	1D Model
$\overline{\dot{V}}_{O_2}$ (mL/min)	271	271
$\overline{\dot{V}}_{CO_2}$ (mL/min)	-272	-267
RQ	1.00	0.99
$\overline{P}_{a,O_2}$ (mmHg)	111.9	114.5
$\overline{P}_{a,CO_2}$ (mmHg)	37.7	38
V_T (L)	0.4	0.4

TABLE 7. 1D vs 0D models in hyperventilation: piecewise constant applied pressure defined by (11) with $T = 2$ s, $P_{insp} = -2.0$ cmH$_2$O, $P_{exp} = 0$ cmH$_2$O, IE $= 0.5$.

Table 6 shows that for another hyperventilation scenario in which the period is small but the inspiratory ratio is large, namely $P_{insp} = -2.0$ cmH$_2$O, $P_{exp} = 0$ cmH$_2$O, IE $= 0.7$, the 1D model predicts higher exchanges than its 0D counterpart. One reason may be that the equilibrium between the alveolar pressures and the blood pressures is reached more rapidly in the 0D problem than in the 1D one.

Finally, in Table 7, both models behave similarly for IE $= 0.5$. This tends to show that to optimize the exchange, for the 0D model a small inspiratory fraction is recommended, which is not the case for the 1D model, for which a larger inspiratory fraction is recommended. Note that in every chosen hyperventilation scenario the exchanges are higher than in the reference case given in Table 1 and Table 4. To investigate more deeply the dependency with respect to the inspiratory fraction, we focus on the blood partial pressure of carbon dioxide for various breathing scenarios with IE varying and the period and amplitude of the applied pressure fixed. We consider a normal breathing scenario and study the differences in predicted exchanges for the 0D model and the 1D model with respect to the inspiratory fraction.

In Fig. 10, below a value $IE_0 \approx 0.25$, the blood partial pressure of carbon dioxide predicted by the 0D model is lower than the one predicted by the 1D model, showing that, on average, the exchanges are higher for the 1D model. In particular, if the target blood partial pressure of carbon dioxide is between 40 and 41 mmHg, then the range of inspiratory fractions is larger for the 1D model than for the 0D one. Moreover, no scenario gives partial pressure below 40mmHg for the 0D model, contrary to the 1D model for which the exchanges are significantly higher for IE $> IE_0$. Thus, for larger inspiratory fraction, the 1D model predicts higher exchanges, whereas for small ones it is the 0D model.

In order to understand whether the difference in the behavior of both models with respect to the inspiratory fraction appears only on average, we consider the time evolution of the carbon dioxide flux over a respiration cycle. We see in Fig. 11 that, when the inspiratory fraction is below IE_0, then the fluxes are greater for the 0D model during the whole period, whereas it is the opposite for

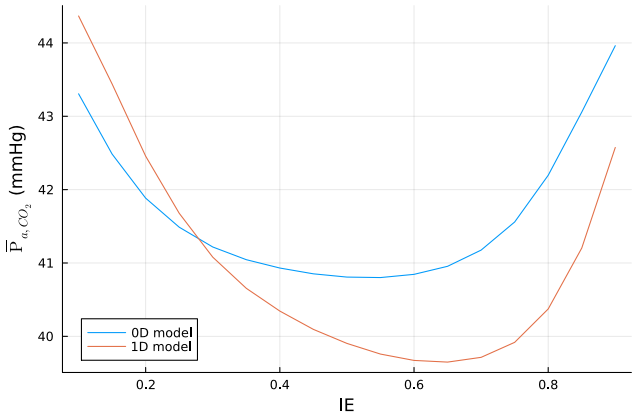

FIGURE 10. $\overline{\mathrm{P}}_{a,\mathrm{CO}_2}$ vs IE for the 1D and 0D models with a piecewise constant applied pressure defined by (11) with $T = 5$ s, $\mathrm{P}_{\mathrm{insp}} = -2.0$ $\mathrm{cmH_2O}$, $\mathrm{P}_{\mathrm{exp}} = 0$ $\mathrm{cmH_2O}$.

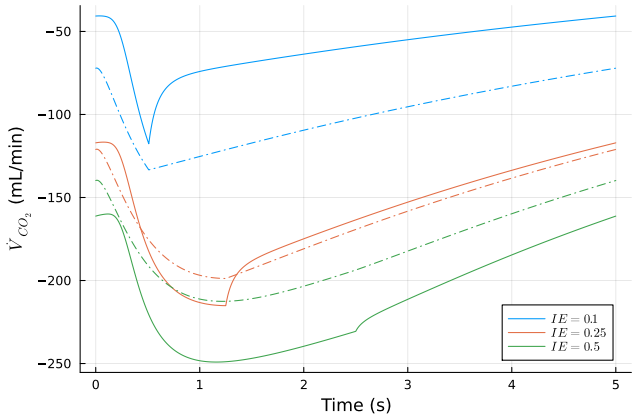

FIGURE 11. Time evolution of $\dot{V}_{\mathrm{CO}_2}$ over a breathing period for three different values of the inspiratory ratio: $IE = 0.1, 0.25, 0.5$. Comparison of the 1D model (plain line) and the 0D model (dash - dot line).

$\mathrm{IE} > \mathrm{IE}_0$. For $\mathrm{IE} = \mathrm{IE}_0$, then the flux $\dot{V}_{\mathrm{CO}_2}$ is greater at the beginning of inspiration for the 0D model, then the exchanges are higher in the 1D case and both models behave similarly at expiration.

3.2.2. *Sensitivity analysis with respect to the breathing scenario.* In this subsection, we investigate the sensitivity of the models with respect to the breathing scenario by making the time period T, the inspiratory pressure $\mathrm{P}_{\mathrm{insp}}$, and the inspiratory fraction IE vary for a healthy case. First, we consider a piecewise constant pattern with $T \in [2.8, 6]$ s, $\mathrm{P}_{\mathrm{insp}} \in [-3, -1]$ $\mathrm{cmH_2O}$ and $\mathrm{IE} \in [0.2, 0.8]$, then a piecewise exponential pattern with $T \in [2.8, 6]$ s, $\mathrm{P}_{\mathrm{insp}} \in [-3.5, -1.5]$ $\mathrm{cmH_2O}$ and $\mathrm{IE} \in [0.2, 0.8]$.

The output variables are the average blood partial pressures of each gas over a time period, namely $\overline{\mathrm{P}}_{a,\mathrm{O}_2}$ and $\overline{\mathrm{P}}_{a,\mathrm{CO}_2}$ given by (15).

In the series of Figures 12-15, 16-19, 20-23 and 24-27 each dot of coordinates $(\overline{\mathrm{P}}_{a,\mathrm{CO}_2}, \overline{\mathrm{P}}_{a,\mathrm{O}_2})$ corresponds to a simulation for the 0D model and 1D model respectively, with piecewise constant or piecewise exponential patterns. These dots are colored with respect to the input parameters, namely T, $|\mathrm{P}_{\mathrm{insp}}|$, IE as well as the work of the applied pressure $\mathcal{W}$ (defined by (16)). Moreover, for each simulation, we zoom in $\overline{\mathrm{P}}_{a,\mathrm{CO}_2} \approx 40$ mmHg; the dots are then represented with correction by the quadratic regression curve.

First, we note that for a given $\overline{\mathrm{P}}_{a,\mathrm{CO}_2}$, the blood partial pressure of oxygen $\overline{\mathrm{P}}_{a,\mathrm{O}_2}$ is fixed in the 0D case. For the 1D case, there is more dispersion but $\overline{\mathrm{P}}_{a,\mathrm{O}_2}$ has small variations around a given value. Thus, both models provide an operating point: for instance for $\overline{\mathrm{P}}_{a,\mathrm{CO}_2} = 40$ mmHg, $\overline{\mathrm{P}}_{a,\mathrm{O}_2} \approx 100$ mmHg, which are the standard values for healthy patients. Yet, there is no unique scenario that gives this point. As a consequence fixing $\overline{\mathrm{P}}_{a,\mathrm{CO}_2}$ or $\overline{\mathrm{P}}_{a,\mathrm{O}_2}$ is not sufficient to discriminate between scenarios and other criteria should be investigated.

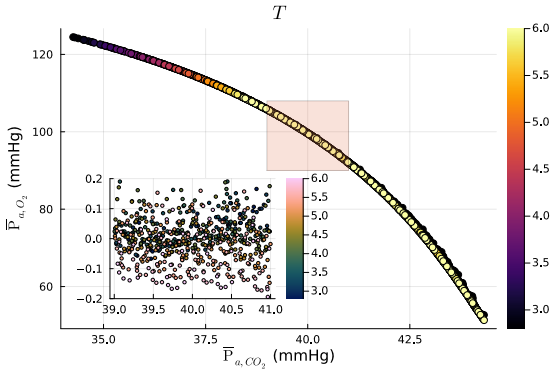

FIGURE 12. $\overline{\mathrm{P}}_{a,\mathrm{O}_2}$ vs $\overline{\mathrm{P}}_{a,\mathrm{CO}_2}$ computed with the 0D model for a timeslot applied pressure. Each dot corresponds to a given scenario and is colored with respect to the time period T.

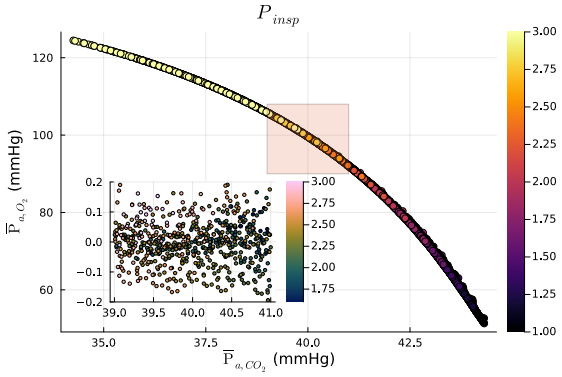

FIGURE 13. $\overline{\mathrm{P}}_{a,\mathrm{O}_2}$ vs $\overline{\mathrm{P}}_{a,\mathrm{CO}_2}$ computed with the 0D model for a timeslot applied pressure. Each dot is colored with respect to inspiratory pressure $\mathrm{P}_{\mathrm{insp}}$.

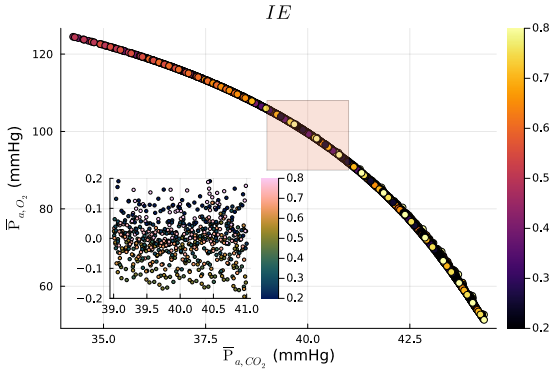

FIGURE 14. $\overline{\mathrm{P}}_{a,\mathrm{O}_2}$ vs $\overline{\mathrm{P}}_{a,\mathrm{CO}_2}$ computed with the 0D model for a timeslot applied pressure. Each dot is colored with respect to inspiratory fraction IE.

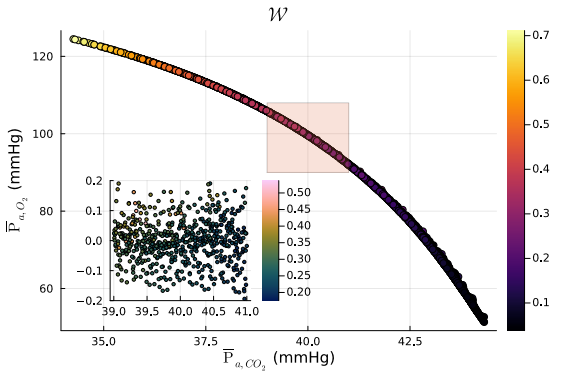

FIGURE 15. $\overline{\mathrm{P}}_{a,\mathrm{O}_2}$ vs $\overline{\mathrm{P}}_{a,\mathrm{CO}_2}$ computed with the 0D model for a timeslot applied pressure. Each dot is colored with respect to the pressure work $\mathcal{W}$.

0D model, piecewise constant applied pressure. For the 0D model, there is no particular pattern with respect to the inspiratory fraction (see Fig. 14), whereas some patterns emerge for the period and are appearing for the inspiratory pressure, as well as for the pressure work. In Fig. 12, for decreasing carbon dioxide blood pressure (and increasing oxygen blood pressure), the average

period decreases: for high gas exchange, the 0D model favors short periods. The $\overline{\mathrm{P}}_{a,\mathrm{O}_2}$–$\overline{\mathrm{P}}_{a,\mathrm{CO}_2}$ curve is even more clearly structured with respect to the inspiratory pressure (see Fig. 13) or the pressure work (see Fig. 15). The general tendency is: the lower the applied pressure, the lower the pressure work and exchange rate.

1D model, piecewise constant applied pressure. Let us now consider the same cases for the 1D model. No structure emerges with respect to T, see Fig. 16, nor IE, see Fig. 18. No tendency appears when $\overline{\mathrm{P}}_{a,\mathrm{CO}_2}$ increases and $\overline{\mathrm{P}}_{a,\mathrm{O}_2}$ decreases. Yet, for a given carbon dioxide blood partial pressure $\overline{\mathrm{P}}_{a,\mathrm{CO}_2}$, the oxygen blood partial pressure $\overline{\mathrm{P}}_{a,\mathrm{O}_2}$ increases as the period decreases. Moreover, when following the curve from left to right in Fig. 17 and Fig.19, on average, $|\mathrm{P}_{\mathrm{insp}}|$ and $\mathcal{W}$ decrease, respectively. Furthermore, for a given carbon dioxide blood pressure $\overline{\mathrm{P}}_{a,\mathrm{CO}_2}$, the oxygen blood pressure $\overline{\mathrm{P}}_{a,\mathrm{O}_2}$ increases as $|\mathrm{P}_{\mathrm{insp}}|$ increases and it comes at the cost of an increase of the pressure work $\mathcal{W}$.

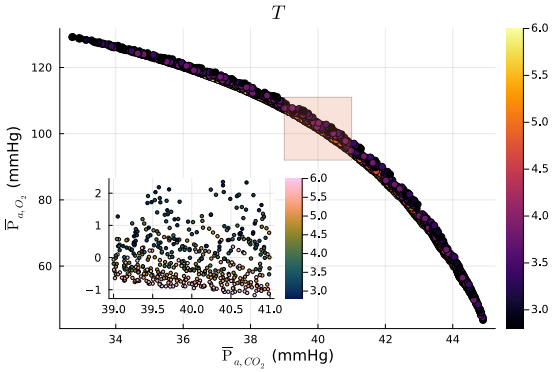

FIGURE 16. $\overline{\mathrm{P}}_{a,\mathrm{O}_2}$ vs $\overline{\mathrm{P}}_{a,\mathrm{CO}_2}$ computed with the 1D model for a timeslot applied pressure. Each dot is colored with respect to the time period T.

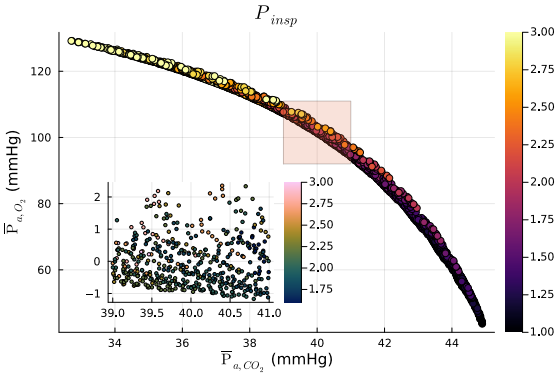

FIGURE 17. $\overline{\mathrm{P}}_{a,\mathrm{O}_2}$ vs $\overline{\mathrm{P}}_{a,\mathrm{CO}_2}$ computed with the 1D model for a timeslot applied pressure. Each dot is colored with respect to the inspiratory pressure $|\mathrm{P}_{\mathrm{insp}}|$.

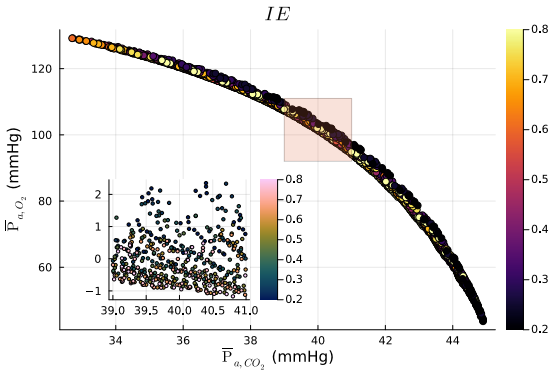

FIGURE 18. $\overline{\mathrm{P}}_{a,\mathrm{O}_2}$ vs $\overline{\mathrm{P}}_{a,\mathrm{CO}_2}$ computed with the 1D model for a timeslot applied pressure. Each dot is colored with respect to the inspiratory IE.

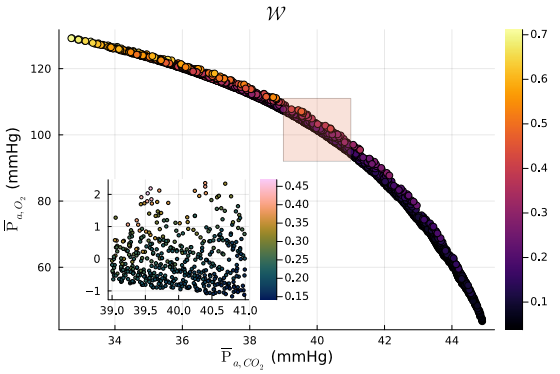

FIGURE 19. $\overline{\mathrm{P}}_{a,\mathrm{O}_2}$ vs $\overline{\mathrm{P}}_{a,\mathrm{CO}_2}$ computed with the 1D model for a timeslot applied pressure. Each dot is colored with respect to the pressure work $\mathcal{W}$.

0D model, piecewise exponential applied pressure. Let us consider the outputs of the 0D model for the piecewise exponential scenario. In Figures 20-23, we observe the same behaviors as the ones observed for the piecewise constant applied pressure, except that for the amplitude of the applied pressure, fewer structures emerge (compare Fig. 21 with Fig. 13). In Fig. 23 we note that a given couple of $(\overline{\mathrm{P}}_{a,\mathrm{CO}_2}, \overline{\mathrm{P}}_{a,\mathrm{O}_2})$ corresponds to a fixed pressure work $\mathcal{W}$. On average, the larger the work, the larger the gas exchanges.

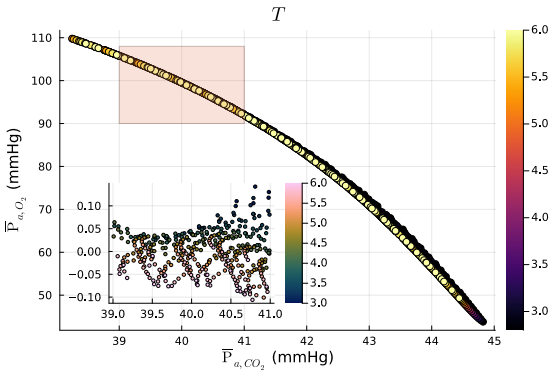

FIGURE 20. $\overline{\mathrm{P}}_{a,\mathrm{O}_2}$ vs $\overline{\mathrm{P}}_{a,\mathrm{CO}_2}$ computed with the 0D Model for a piecewise exponential applied pressure. Each dot is colored with respect to the period T.

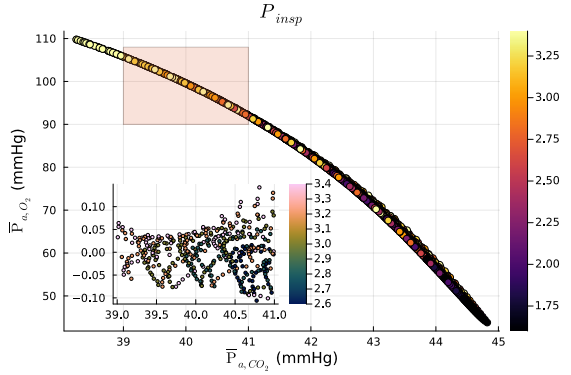

FIGURE 21. $\mathrm{P}_{a,\mathrm{O}_2}$ vs $\mathrm{P}_{a,\mathrm{CO}_2}$ computed with the 0D Model for a piecewise exponential applied pressure. Each dot is colored with respect to the inspiratory pressure $|\mathrm{P}_{\mathrm{insp}}|$.

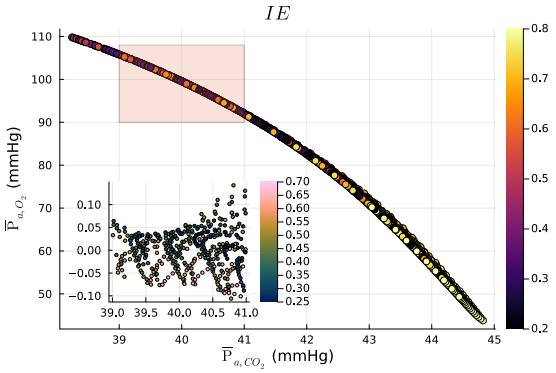

FIGURE 22. $\overline{\mathrm{P}}_{a,\mathrm{O}_2}$ vs $\overline{\mathrm{P}}_{a,\mathrm{CO}_2}$ computed with the 0D Model for a piecewise exponential applied pressure. Each dot is colored with respect to the inspiratory fraction IE

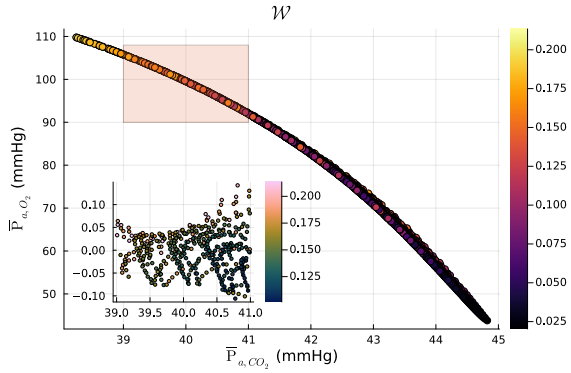

FIGURE 23. $\overline{\mathrm{P}}_{a,\mathrm{O}_2}$ vs $\overline{\mathrm{P}}_{a,\mathrm{CO}_2}$ computed with the 0D Model for a piecewise exponential applied pressure. Each dot is colored with respect to the pressure work $\mathcal{W}$.

1D model, piecewise exponential applied pressure. Finally, let us consider the outputs of the 1D model for the piecewise exponential scenario. The observations are quite similar to the ones made previously: there is no pattern with respect to the inspiratory fraction IE (see Fig. 26), for a fixed carbon dioxide blood partial pressure $\overline{\mathrm{P}}_{a,\mathrm{CO}_2}$ any period will give an oxygen blood partial pressure $\overline{\mathrm{P}}_{a,\mathrm{O}_2}$ slightly varying around a given value, $\overline{\mathrm{P}}_{a,\mathrm{O}_2}$ increasing when the period T decreases

(see Fig. 24). Regarding the amplitude of the inspiratory pressure, the general tendency is, that the larger $|\mathrm{P}_{\mathrm{insp}}|$ is, the larger the gas exchanges are, as shown in Fig. 25. As before and as observed in Fig. 27 the curve remains structured with respect to the pressure work.

From these observations, in particular in the 1D case, if we have a target $\overline{\mathrm{P}}_{a,\mathrm{CO}_2}$ then the $\overline{\mathrm{P}}_{a,\mathrm{O}_2}$ is almost fixed and if we want to minimize the applied pressure work $\mathcal{W}$ then a period T is picked up but several values of the inspiratory fraction IE and amplitude of pressure $|\mathrm{P}_{\mathrm{insp}}|$ may be admissible.

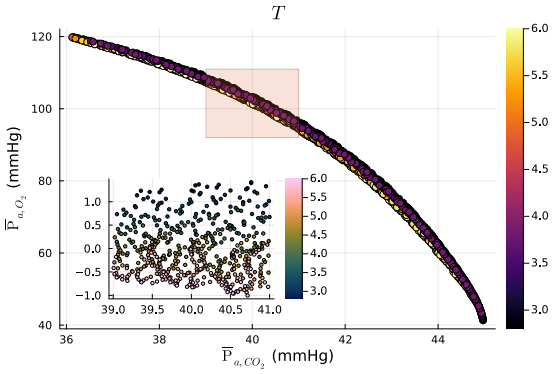

FIGURE 24. $\overline{\mathrm{P}}_{a,\mathrm{O}_2}$ vs $\overline{\mathrm{P}}_{a,\mathrm{CO}_2}$ computed with the 1D Model for a piecewise exponential applied pressure. Each dot is colored with respect to the period T.

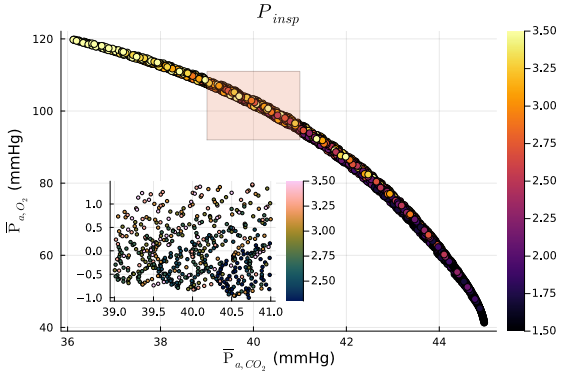

FIGURE 25. $\overline{\mathrm{P}}_{a,\mathrm{O}_2}$ vs $\overline{\mathrm{P}}_{a,\mathrm{CO}_2}$ computed with the 1D Model for a piecewise exponential applied pressure. Each dot is colored with respect to $|\mathrm{P}_{\mathrm{insp}}|$.

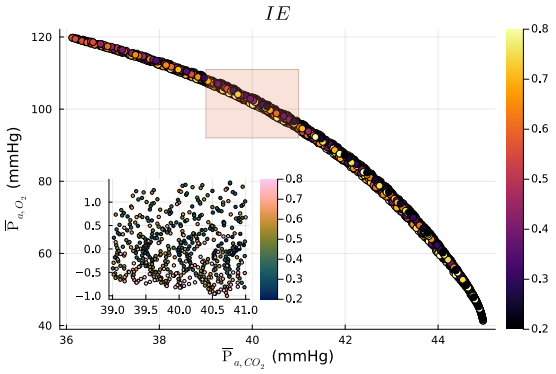

FIGURE 26. $\overline{\mathrm{P}}_{a,\mathrm{O}_2}$ vs $\overline{\mathrm{P}}_{a,\mathrm{CO}_2}$ computed with the 1D Model for a piecewise exponential applied pressure. Each dot is colored with respect to IE.

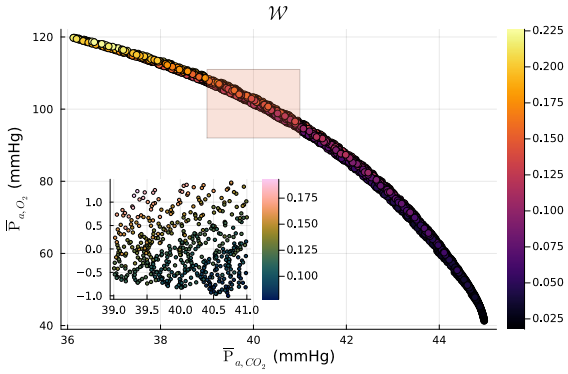

FIGURE 27. $\overline{\mathrm{P}}_{a,\mathrm{O}_2}$ vs $\overline{\mathrm{P}}_{a,\mathrm{CO}_2}$ computed with the 1D Model for a piecewise exponential applied pressure. Each dot is colored with respect to $\mathcal{W}$.

Thus, from these curves, it is unclear why the observed stereotypical scenario corresponds to an inspiratory fraction of 0.4. The aim of the next section is to explore which cost function could select the particular scenario observed in practice.

3.3. **Optimal breathing scenario.** Now, let us investigate which cost function the observed standard breathing scenario is minimizing. As we already mentioned, there exist chemical sensors in the brain that measure the carbon dioxide blood partial pressure [16, 22]. Thus, the respiratory

breathing pattern may adapt to maintain this partial pressure at a given level or in a given interval. In the case of our models, a given carbon dioxide blood partial pressure corresponds to a fixed oxygen blood partial pressure. Yet, as noted in the previous subsection, neither in the 0D case, nor in the 1D case, any particular scenario is selected, since there is no uniqueness of the scenario that provides a given output. Furthermore, minimizing the applied pressure work is not sufficient to discriminate between several scenarios. Consequently, as there are mechanical captors that are sensible to the lung elongation during inspiration [22], we consider an additional criterion which measures the difference between the maximal inhaled volume and the standard functional residual capacity, namely $\mathcal{D}_V = (V_{\max} - V_{\mathrm{FRC}})^2$. As in the previous subsection, we consider four cases: the 0D model and the 1D model both for piecewise constant and piecewise exponential applied pressure. In the obtained series of Figures 28-30, 31-33, 34-36 and 37-39, the point of coordinates $(\mathcal{D}_V, W)$ corresponds to one model and a fixed breathing scenario and each dot is colored with respect to the period T, the inspiratory pressure amplitude $|\mathrm{P}_{\mathrm{insp}}|$ or the inspiratory fraction IE associated with the specific scenario. We keep only the simulations for which the carbon dioxide blood partial pressure $\overline{\mathrm{P}}_{a,\mathrm{CO}_2}$ belongs to the range $[39, 41]$ mmHg.

0D model, piecewise constant applied pressure. In Fig. 28, 29,and 30, the inputs that minimize both $\mathcal{D}_V$ and $\mathcal{W}$ among the simulations performed correspond to small periods (around 3 s), small amplitudes and rather small inspiratory fractions. These values do not correspond to the standard breathing scenario. Note that for the performed test cases, as $|\mathrm{P}_{\mathrm{insp}}|$ increases, $\mathcal{D}_V$ and $\mathcal{W}$ increase as well.

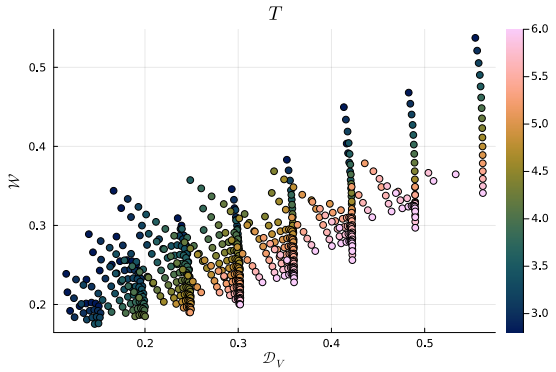

FIGURE 28. $\mathcal{W}$ vs $\mathcal{D}_V$ computed with the 0D model for a timeslot applied pressure. Each dot is colored with respect to the time period T.

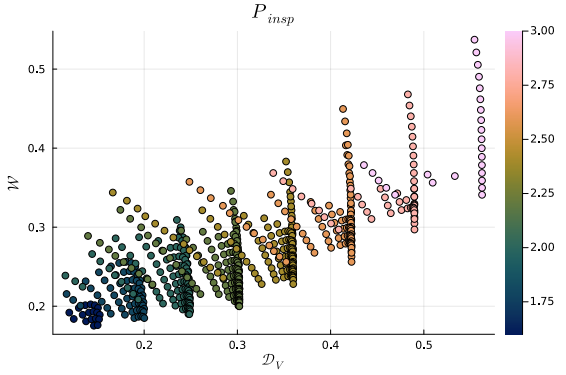

FIGURE 29. $\mathcal{W}$ vs $\mathcal{D}_V$ computed with the 0D model for a timeslot applied pressure. Each dot is colored with respect to the inspiratory pressure $\mathrm{P}_{\mathrm{insp}}$.

1D model, piecewise constant applied pressure. In Fig. 31, 32, and 33, we observe that, among the performed test cases, the scenario which gives the smallest values of $\mathcal{W}$ and $\mathcal{D}_V$ is not the same as for the 0D case. The selected inspiratory fraction and period are larger than in the 0D case and, in particular, it seems to select a value of IE around 0.7, which is large compared to the standard value of 0.4. As for the 0D model, we observe that $\mathcal{W}$ and $\mathcal{D}_V$ are correlated to $\mathrm{P}_{\mathrm{insp}}$.

0D model, piecewise exponential applied pressure. By considering the 0D model for various piecewise exponential scenarios, we observe in Fig. 35 and Fig. 36 that, once again, to have the smallest values of $\mathcal{W}$ and $\mathcal{D}_V$ one has to select small inspiratory fraction IE (yet larger than in the piecewise constant case), and small inspiratory pressure $|\mathrm{P}_{\mathrm{insp}}|$. Note that this inspiratory pressure is larger than the one in the piecewise constant scenario. This can be explained by the pressure pattern and the need to sufficiently ventilate the lung to obtain a carbon dioxide blood partial

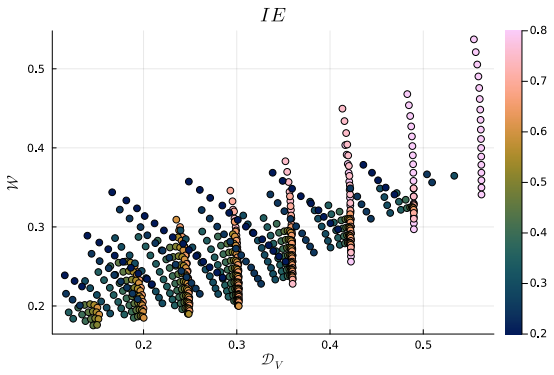

FIGURE 30. $\mathcal{W}$ vs $\mathcal{D}_V$ computed with the 0D model for a timeslot applied pressure. Each dot is colored with respect to the inspiratory fraction IE.

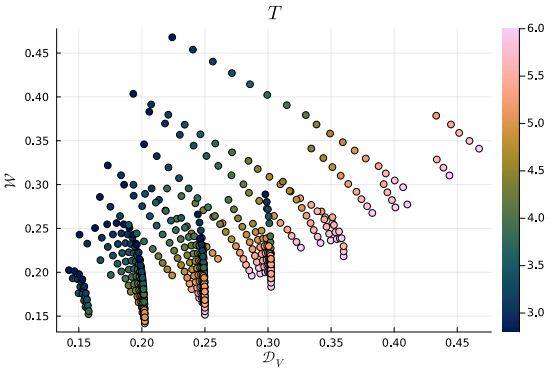

FIGURE 31. $\mathcal{W}$ vs $\mathcal{D}_V$ computed with the 1D model for a timeslot applied pressure. Each dot are colored with respect to the time period T.

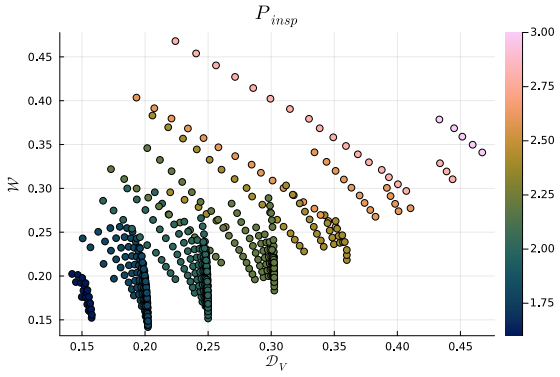

FIGURE 32. $\mathcal{W}$ vs $\mathcal{D}_V$ computed with the 1D model for a timeslot applied pressure. Each dot are colored with respect to the inspiratory pressure $\mathrm{P}_{\mathrm{insp}}$.

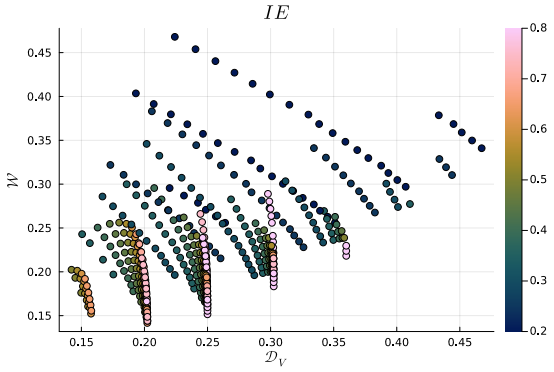

FIGURE 33. $\mathcal{W}$ vs $\mathcal{D}_V$ computed with the 1D model for a timeslot applied pressure. Each dot are colored with respect to the inspiratory fraction IE.

pressure $\overline{\mathrm{P}}_{a,\mathrm{CO}_2}$ in the range $[39, 41]$ mmHg. Note moreover that the period for small $\mathcal{W}$ and $\mathcal{D}_V$ in Fig. 34 is larger than the one for the piecewise constant scenario described in Fig. 28.

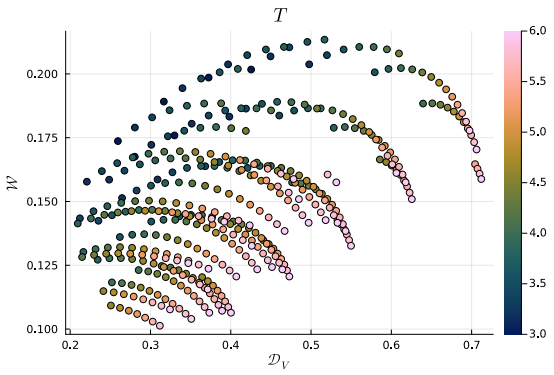

FIGURE 34. 0D Model $\mathcal{W}$ vs $\mathcal{D}_V$ for a piecewise exponential pressure, colored with respect to the period T.

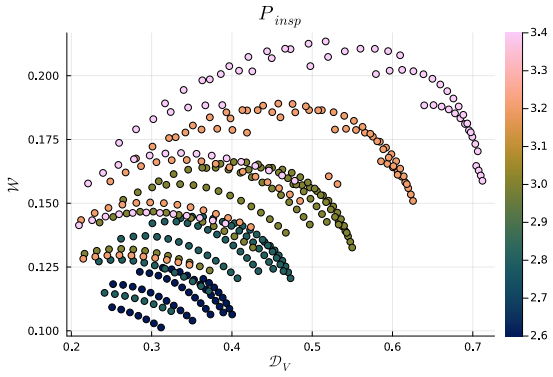

FIGURE 35. 0D Model $\mathcal{W}$ vs $\mathcal{D}_V$ for a piecewise exponential pressure, colored with respect to the inspiratory pressure $|\mathrm{P_{insp}}|$.

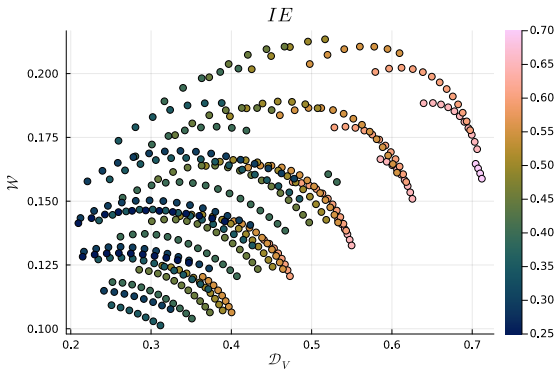

FIGURE 36. 0D Model $\mathcal{W}$ vs $\mathcal{D}_V$ for a piecewise exponential pressure, colored with respect to the inspiratory fraction IE.

1D model, piecewise exponential applied pressure. Finally in Fig. 37, 38, 39 where we consider the 1D model for various exponential piecewise scenarios, we observe that, to obtain the smallest values of $\mathcal{W}$ and $\mathcal{D}_V$, the period is around 5 s and the inspiratory fraction is higher than in the 0D case and close to the desired value of 0.4. This was not the case for the 1D model with a piecewise constant scenario which favors a larger inspiratory fraction.

Optimal breathing pattern. Next, in order to focus on the scenarios that optimize the applied pressure work $\mathcal{W}$ without stretching the lung too much, we select the ten best scenarios in the following sense: we choose the following cost function, $\alpha\mathcal{D}_V^2 + \beta\mathcal{W}^2$ where we choose to normalize both components in order to obtain the same order of magnitude. Note that this normalization depends on the considered range of parameters used in our test cases. Tables 8-11 gather together the average and standard deviation of the input data T, $\mathrm{P_{insp}}$, IE and output data $\overline{\mathrm{P}}_{a,\mathrm{CO_2}}$, $\overline{\mathrm{P}}_{a,\mathrm{O_2}}$, V_T of the ten best scenarios with different target for the carbon dioxide blood partial pressure $\overline{\mathrm{P}}_{a,\mathrm{CO_2}}$. In Table 8, we consider only the $\overline{\mathrm{P}}_{a,\mathrm{CO_2}}$ between 39 and 41 mmHg for a piecewise constant applied pressure. The main differences between the 0D and 1D case are that the period and the inspiratory fraction are smaller in the 0D case. Neither model provides expected in terms of period, inspiratory fraction and tidal volume even if they provide standard values for the blood partial pressures. Next, considering the scenarios for which the cost function is minimal (among the performed simulations)

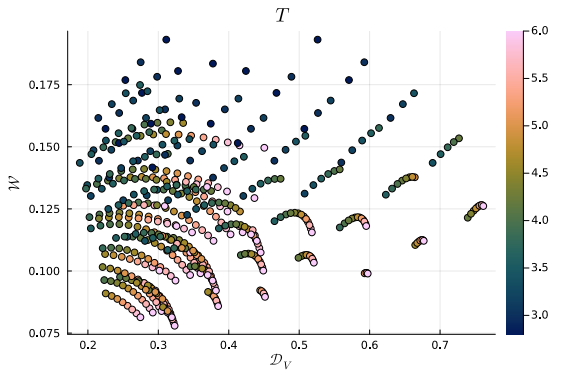

FIGURE 37. 1D Model $\mathcal{W}$ vs $\mathcal{D}_V$ for a piecewise exponential pressure, colored with respect to the period T.

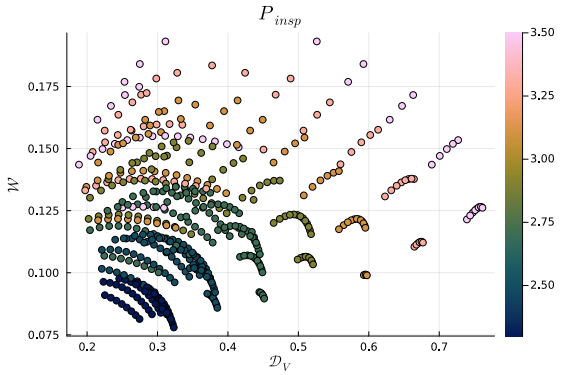

FIGURE 38. 1D Model $\mathcal{W}$ vs $\mathcal{D}_V$ for a piecewise exponential pressure, colored with respect to the inspiratory pressure $|\mathrm{P_{insp}}|$.

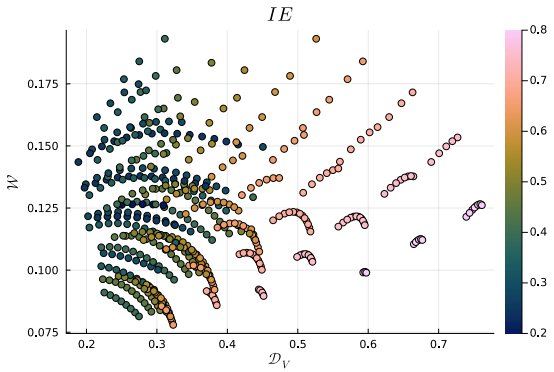

FIGURE 39. 1D Model $\mathcal{W}$ vs $\mathcal{D}_V$ for a piecewise exponential pressure, colored with respect to the inspiratory fraction IE.

	0D Model	1D Model
T (s)	3.10 ± 0.22	3.64 ± 0.21
$\mathrm{P_{insp}}$ (cmH2O)	-1.64 ± 0.08	-1.6 ± 0.0
IE	0.38 ± 0.08	0.59 ± 0.05
$\overline{\mathrm{P}}_{a,\mathrm{CO_2}}$ (mmHg)	40.84 ± 0.14	40.89 ± 0.06
$\overline{\mathrm{P}}_{a,\mathrm{O_2}}$ (mmHg)	93.42 ± 1.10	96.15 ± 0.63
V_T (L)	0.36 ± 0.01	0.37 ± 0.01
$\mathcal{W}$ ($\mathrm{cmH_2O \cdot L \cdot s^{-1}}$)	0.19 ± 0.01	0.16 ± 0.01
$\mathcal{D}_V$ ($\mathrm{L^2}$)	0.13 ± 0.01	0.16 ± 0.01

TABLE 8. Selected mean scenario with timeslot pressure for a $\overline{\mathrm{P}}_{a,\mathrm{CO_2}}$ between 39 and 41 mmHg

and for which $\overline{\mathrm{P}}_{a,\mathrm{CO_2}}$ is smaller than 40 mmHg, we observe in Table 9 that we have the same type of scenarios but with an average value of $\overline{\mathrm{P}}_{a,\mathrm{O_2}}$ higher than previously. This is not surprising since we select simulations for which $\overline{\mathrm{P}}_{a,\mathrm{CO_2}} \leq 40$ and thus, possibly, better gas exchanges than in the case where $\overline{\mathrm{P}}_{a,\mathrm{CO_2}} \in [39, 41]$.

	0D Model	1D Model
T (s)	3.02 ± 0.18	3.82 ± 0.15
$\mathrm{P}_{\mathrm{insp}}$ (cmH2O)	-1.82 ± 0.06	-1.8 ± 0.0
IE	0.41 ± 0.08	0.60 ± 0.07
$\overline{\mathrm{P}}_{a,\mathrm{CO}_2}$ (mmHg)	39.82 ± 0.14	39.84 ± 0.11
$\overline{\mathrm{P}}_{a,\mathrm{O}_2}$ (mmHg)	100.77 ± 0.89	103.03 ± 0.62
V_T (L)	0.40 ± 0.01	0.42 ± 0.01
$\mathcal{W}$ ($\mathrm{cmH_2O \cdot L \cdot s^{-1}}$)	0.24 ± 0.01	0.20 ± 0.01
$\mathcal{D}_V$ (L^2)	0.17 ± 0.02	0.20 ± 0.01

TABLE 9. Selected mean scenario with timeslot pressure for a $\overline{\mathrm{P}}_{a,\mathrm{CO}_2}$ under 40 mmHg

	0D Model	1D Model
T (s)	5.08 ± 0.41	5.06 ± 0.67
$\mathrm{P}_{\mathrm{insp}}$ (cmH2O)	-2.66 ± 0.10	-2.30 ± 0.0
IE	0.34 ± 0.02	0.41 ± 0.02
$\overline{\mathrm{P}}_{a,\mathrm{CO}_2}$ (mmHg)	40.91 ± 0.03	40.92 ± 0.05
$\overline{\mathrm{P}}_{a,\mathrm{O}_2}$ (mmHg)	92.76 ± 0.28	95.37 ± 0.53
V_T (L)	0.51 ± 0.03	0.47 ± 0.03
$\mathcal{W}$ ($\mathrm{cmH_2O \cdot L \cdot s^{-1}}$)	0.11 ± 0.01	0.09 ± 0.01
$\mathcal{D}_V$ (L^2)	0.27 ± 0.02	0.25 ± 0.02

TABLE 10. Selected mean scenario with piecewise exponential pressure for a $\overline{\mathrm{P}}_{a,\mathrm{CO}_2}$ between 39 and 41 mmHg

	0D Model	1D Model
T (s)	4.96 ± 0.48	5.08 ± 0.64
$\mathrm{P}_{\mathrm{insp}}$ (cmH2O)	-2.90 ± 0.14	-2.50 ± 0.0
IE	0.41 ± 0.06	0.46 ± 0.02
$\overline{\mathrm{P}}_{a,\mathrm{CO}_2}$ (mmHg)	39.91 ± 0.05	39.88 ± 0.08
$\overline{\mathrm{P}}_{a,\mathrm{O}_2}$ (mmHg)	100.14 ± 0.36	102.57 ± 0.53
V_T (L)	0.58 ± 0.03	0.52 ± 0.04
$\mathcal{W}$ ($\mathrm{cmH_2O \cdot L \cdot s^{-1}}$)	0.14 ± 0.01	0.11 ± 0.01
$\mathcal{D}_V$ (L^2)	0.37 ± 0.04	0.32 ± 0.02

TABLE 11. Selected mean scenario with piecewise exponential pressure for a $\overline{\mathrm{P}}_{a,\mathrm{CO}_2}$ under 40 mmHg

Next, we present the same results for the case of a piecewise exponential applied pressure. We observe in Tables 10 and 11 that the selected scenario in the 1D case corresponds almost to the commonly accepted standard values, both for the inputs and the outputs. This is not the case for the 0D model, for which IE is still below the expected value in the case where the $\overline{\mathrm{P}}_{a,\mathrm{CO}_2}$ is between 39 and 41 mmHg.

Let us now change the cost function by adding a constraint on $\overline{\mathrm{P}}_{a,\mathrm{CO}_2}$ in order to minimize its distance to 40 mmHg. The new considered cost function is the same as before but we add the term $(\overline{\mathrm{P}}_{a,\mathrm{CO}_2} - 40)^2$. Note here that this term is not normalized like the other two, since we want to put a greater weight on this criterion. Tables 12 and 13 show, again, that, for a piecewise constant pressure, the selected IE is lower than the standard value for the 0D model and larger for the 1D model. Note moreover that the tidal volume is lower than the standard value. In the case of a piecewise exponential applied pressure we obtain a strong good fit with the standard values for the

	0D Model	1D Model
T (s)	3.10 ± 0.25	3.94 ± 0.27
$\mathrm{P}_{\mathrm{insp}}$ (cmH2O)	-1.84 ± 0.08	-1.8 ± 0.0
IE	0.36 ± 0.08	0.61 ± 0.09
$\overline{\mathrm{P}}_{a,\mathrm{CO}_2}$ (mmHg)	40.03 ± 0.12	40.00 ± 0.07
$\overline{\mathrm{P}}_{a,\mathrm{O}_2}$ (mmHg)	99.41 ± 0.80	102.08 ± 0.56
V_T (L)	0.40 ± 0.02	0.42 ± 0.01
$\mathcal{W}$ ($\mathrm{cmH_2O \cdot L \cdot s^{-1}}$)	0.23 ± 0.02	0.19 ± 0.01
$\mathcal{D}_V$ (L^2)	0.16 ± 0.02	0.20 ± 0.01

TABLE 12. Selected mean scenario with timeslot pressure with modified functional: the cost function is penalized by $(\overline{\mathrm{P}}_{a,\mathrm{CO}_2} - 40)^2$.

	0D Model	1D Model
T (s)	5.00 ± 0.52	5.10 ± 0.61
$\mathrm{P}_{\mathrm{insp}}$ (cmH2O)	-2.82 ± 0.06	-2.50 ± 0.0
IE	0.39 ± 0.02	0.42 ± 0.03
$\overline{\mathrm{P}}_{a,\mathrm{CO}_2}$ (mmHg)	40.09 ± 0.10	40.10 ± 0.12
$\overline{\mathrm{P}}_{a,\mathrm{O}_2}$ (mmHg)	98.93 ± 0.69	101.21 ± 0.78
V_T (L)	0.57 ± 0.04	0.52 ± 0.04
$\mathcal{W}$ ($\mathrm{cmH_2O \cdot L \cdot s^{-1}}$)	0.13 ± 0.01	0.10 ± 0.01
$\mathcal{D}_V$ (L^2)	0.35 ± 0.03	0.30 ± 0.03

TABLE 13. Selected mean scenario with piecewise exponential pressure with modified functional: the cost function is penalized by $(\overline{\mathrm{P}}_{a,\mathrm{CO}_2} - 40)^2$.

1D model, which is not the case of the 0D model, where the tidal volume is larger and thus the associated pressure work is larger than the one obtained in the 1D case.

4. Discussions

Let us now comment on the obtained results compared to previous works, on the importance of modeling the time delay and its impact on the optimal cost function and the recovery of an optimal scenario. We also conclude this section by addressing the limitations of the model and its possible extensions for clinical use.

4.1. **Models comparison with previous works.** Several authors have considered similar 1D models, most of which consider oxygen alone [33, 43, 37, 24]. In [29] the oxygen and carbon dioxide are taken into account. We shall emphasize that there are some differences between the parameters chosen in our model and those considered in [29]. The geometry is different since in [29] a homothetic geometry is chosen (each generation's length and radius is obtained by a geometric law from the morphometry of the trachea) which gives a different length and radius distribution along the tree and thus different surface exchange. Here our geometry is based on morphometric data and is similar to the one considered in [24]. The second main difference in the parameters is the gas diffusion coefficient through the alveolo-capillary membrane. In [29], its value was chosen much higher than in our simulations, leading to, possibly, overestimate the gas exchanges. As a consequence the given deoxygenated blood partial pressures of gases $\mathrm{P}_{v,\mathrm{gas}}$ were fitted in order to recover good orders of magnitude of the output data. These pressures were seen as the pressures of a mixture of deoxygenated and oxygenated blood, surely to counterbalance the high diffusion coefficient between alveolar and blood partial pressures that tends to overestimate the gas fluxes. Contrary to [29] we recover the standard average values of the outputs without any fitting and using

the standard values of the parameters in our model. Moreover, the 1D outputs along the tree for oxygen are similar to those obtained in [24] or [43] which consider the oxygen diffusion only. The oxygen and carbon dioxide concentrations along the tree are also similar to those obtained in [29].

Furthermore, we have observed that, both at rest and for moderate exercise, the main part of the gas exchanges takes place at the tree terminals as in [43, 24], but contrary to [37, 29], where, at rest, the distal region is not involved in gas exchanges whereas it is involved at exercise. In [37, 29], the authors attribute this feature of their model to the *so-called* screening effect. Here the capacity of our model to maintain good gas exchanges at exercise results from the increase of the blood capillary volume in accordance with [13]. The difference between our model and the ones proposed in [37, 29] lies in the modeling of the reaction term and gas exchange through the alveolo-capillary membrane. In [37, 29] the authors introduce an effective diffusion coefficient, whereas here as in [43], the gas fluxes are computed by solving a 0D system based on the gas exchange dynamics, at each time step, leading to a sharp and accurate estimate of the gas exchanges. Moreover, this 0D system allows us to have a robustness in the gas exchanges regarding the diffusing capacity D_m as seen with the sensitivity analysis (see Table 2). Indeed, the parameter D_m can be slightly modified without affecting the gas exchanges with the blood.

4.2. **Time delay.** Contrary to the 1D model, the 0D model does not take into account the transit time of air through the bronchial tree which induces a time delay due to the transport and the mixing of gases in the dead space region. However, note that for both chosen normal breathing scenarios, the 1D model predicts higher gas exchange. One reason may be that the time delay is beneficial to maintain higher exchanges on average over a time period by maintaining a difference between the alveolar pressures and blood pressures. It could be in particular due to the fact that, at expiration, the gases stay longer in the acinar region enabling higher exchanges: the advection-diffusion 1D model naturally takes into account the time delay and mixing of gases in the bronchial tree.

Moreover, the influence of the time delay is further observed by making the inspiratory fraction vary: for larger inspiratory fraction, the 1D model predicts higher exchanges whereas, for smaller ones, the higher exchanges are predicted with the 0D model. This may be explained by the transit time in the bronchial tree: for small inspiratory fraction, fresh air fails to reach the acini and for large inspiratory fractions, the 0D model equilibrium more rapidly between alveolar and blood pressures, minimizing the fluxes through the alveolo-capillary membrane and the gas exchanges.

Furthermore, one key feature of our model is that it is driven by an applied pressure (contrary to [43, 29] which imposed a given fluid flow) enabling the study of its impact on the gas transport and diffusion. Concerning the two considered breathing scenarios, we thus observe a difference in time delay. Indeed, there is a larger time delay with the exponential pattern. This is due to the fact that with a piecewise constant scenario, the airflow in the tree at beginning of the inspiration and at the beginning of the expiration is much larger than with the piecewise exponential scenario. This allows the oxygenated air to reach the alveoli much quicker and thus the exchanges take place earlier in the breathing cycle. The carbon dioxide-filled air is also expelled rapidly which allows the lung to come back to its resting state (V_{FRC}) earlier in the breathing cycle. To some extent, the delay seems to be beneficial to enhance gas exchanges.

4.3. **Optimal breathing.** The time delay also influences the sensitivity of the models with respect to the optimality of the standard reference breathing scenario. In particular, the differences in the optimal ventilation between the 0D case and the 1D case for the piecewise constant scenario may be explained by the transit time induced by the bronchial tree: the 1D model cannot ensure enough gas exchanges when the period, the inspiratory pressure and the inspiratory ratio are small, whereas the 0D model allows the exchanges to take place without time delay. This could explain the difference between the optimal inspiratory fraction in the 0D case and the 1D case for the piecewise

constant scenario. The difference is reduced for the piecewise exponential scenario since a time delay is already taken into account with the breathing scenario.

We have also observed that many scenarios provide a target couple $(\overline{\mathrm{P}}_{a,\mathrm{O}_2}, \overline{\mathrm{P}}_{a,\mathrm{CO}_2})$, since when $\overline{\mathrm{P}}_{a,\mathrm{CO}_2}$ is fixed so is $\overline{\mathrm{P}}_{a,\mathrm{O}_2}$, ensuring robustness in the respiratory process. Yet, to select the acknowledged standard breathing features (period, inspiratory ratio, inspiratory pressure) the cost function to minimize should take into account not only the respiratory work but also the lung distension and a target carbon dioxide blood partial pressure. Indeed, minimizing the respiratory work together with a carbon dioxide blood partial pressure target tends to select large inspiratory fraction (IE > 0.6). It implies that the lung has less time to come back to its resting state (V_{FRC}) and that the end-expiratory volume is greater than V_{FRC}, which results in a more significant elongation of the lung. This may explain why the lung distension is an important criterion in selecting optimal breathing. On the other hand, if we only consider lung distension in the cost function together with a carbon dioxide blood partial pressure target, it tends to select small inspiratory fractions ($IE < 0.3$) (in this case, to ensure good exchanges, the applied pressure is large and thus the breathing work is also). Indeed, with smaller inspiratory fractions, the lung has time to return to its resting state, so the distension is less significant. Thus, the lung distension and respiratory work are both to be considered to correctly select the various parameters (especially the inspiratory fraction) needed to obtain the standard applied pressure features. In [29], the authors minimized the respiratory work with an oxygen flux constraint where only the breathing period and air flux amplitude were to be fitted while the inspiratory fraction was fixed at 0.5. Here, the exhibited minimization problem both better mimics the physiology, since there exist lung distension and carbon dioxide sensors, and enables us to recover standard breathing patterns. Yet, in pathological situations, these considered cost functions may be insufficient and one may have to enrich them to take into account, for instance, an oxygen blood partial pressure as an objective (here it is not necessary since to a given carbon dioxide partial pressure corresponds an almost unique oxygen blood partial pressure).

4.4. **Model limitations.** The proposed model has several notable limitations that warrant consideration. Firstly, it relies on a simplified representation of the bronchial tree and alveolar region, overlooking the heterogeneity of the alveolar region [36], including the acini and alveolar ducts. The assumption of symmetric branching in our 1D model serves as a minimal baseline that allows tractable computations. Although real pulmonary trees exhibit local asymmetries, especially in branch length and diameter [41, 48], the overall architecture of the bronchial tree follows a highly repetitive and quasi-symmetric structure, particularly in the conducting zones. Thus, symmetric branching offers a simplified yet biologically grounded representation of the structure, and enables us to derive analytical insights into flow distribution and gas transport efficiency. Note that the symmetry assumption may be partially relaxed, for instance when using different 1D distal subtrees connected to a 3D proximal tree, see [30, 32]. This may be a future direction of work as the inclusion of airway asymmetry is critical for capturing heterogeneities in aerosol transport and deposition, as well as for modeling the spatially localized development of obstructive or inflammatory lung conditions.

Moreover, the model does not consider the possible effects of ventilation-perfusion mismatch [22, 49], a factor that can be significant in understanding and treating various pathological conditions. The perfusion of the lung by the heart is taken into account in our model by the capillary volume V_c and the transit time τ_b, which we could consider as dependent on the lung generation or, as just mentioned, this ventilation-perfusion mismatch could also be modelled by considering several 1D connected subtrees.

Additionally, it is known that gravity affects ventilation: the lower regions of the lung are better ventilated than the upper regions because of the effects of gravity on the lung [49]. Here, we do not account for these potential effects.

The description of gas exchange across the alveolar-capillary membrane is also simplified and relies on phenomenological laws that may not capture the full complexity of the process. One could develop more realistic dynamical systems for instance based on chemical equilibrium as in [23] in a steady state context.

Let us emphasize furthermore that we have chosen to focus only on the respiratory process and to consider the control of ventilation as an optimal control problem, omitting the coupling with other organs such as the heart, the kidneys and the brain (as in [5], which considers complex coupled 0D dynamical systems) and the control of the respiratory system as a feedback control [10, 15, 39].

4.5. **Towards clinical understanding.** We have demonstrated the ability of the 1D model to recover:

- a realistic behavior both at rest and during exercise using physiological parameters in a healthy case;
- a realistic CO_2 washout curve;
- an acknowledged breathing scenario with $T = 5$ s and $\mathrm{IE} = 0.4$, by considering a well-chosen cost function that minimizes respiratory work, lung distension, and targets a carbon dioxide blood partial pressure.

Thus, this model has been validated in healthy cases, and it could be used to model different diseases. Indeed, we can assume that lung diseases can be taken into account by modifying some of the model's parameters. For example, as in the study performed in the 0D case in [7], asthma can be modelled thanks to an increase in airway resistance R, emphysema by a decrease in lung elastance E, and fibrosis by an increase in E. These parameter modifications can then be integrated into the 1D model to simulate the effects of these diseases on gas exchanges and ventilation. Note, however, that, for asthma, modifying only R is not sufficient and one should modify the geometry of the bronchial tree accordingly. Adapting our model to pathologies would allow for a better understanding of pathophysiological mechanisms and better adaptation of treatments.

Furthermore, the model could be used to optimize mechanical ventilation by adapting the ventilator's settings to the patient's needs in order to optimize oxygen delivery and minimize lung damage, which is a major drawback of mechanical ventilation [9]. In particular, as demonstrated, the piecewise constant pressure applied by mechanical ventilators may not be optimal in the considered scenarios. The exponential pleural pressure applied seems to favor gas exchanges with lower lung extension and lower applied pressure work, which could induce fewer lung injuries.

5. Conclusion and perspectives

We have presented a new 1D-0D coupled system developed to describe the transport and diffusion of oxygen and carbon dioxide in the bronchial tree and through the blood. This model is a coupled non-linear model that enables us to recover acknowledged standard values of gas fluxes and blood partial pressures without any fitting of the input physiological parameters. This model naturally takes into account the time delay induced by the air transport along the bronchial tree.

We have compared it to its 0D counterpart. For standard breathing scenarios, it appears that the time delay favors gas exchange. This can be explained by the fact that, for the 0D model, the equilibrium between alveolar pressures and blood pressures is reached more rapidly, whereas the transport in the bronchial tree maintains a gap between the alveolar and blood partial pressures.

We have also investigated the sensitivity of both models with respect to breathing scenarios by considering two types of pleural applied pressure: a piecewise constant and a piecewise exponential (modeling the action of the respiratory muscles). As no time delay is modelled in the 0D model, the physiological gas exchanges can be reached for small breathing period, small inspiratory ratio, and small inspiratory pressure amplitude. It is not the case for the 1D model, for which the period and the inspiratory ratio have to be larger. Furthermore, for both models, we have observed that a given carbon dioxide arterial partial pressure is associated with a unique or almost unique oxygen arterial

partial pressure. However, numerous scenarios provide these pairs. This non-uniqueness makes the breathing process quite robust with respect to the breathing pattern; yet it leads to a natural question: which criteria enable to select a particular breathing pattern? To answer this question, we have explored several cost functions: the pressure work, the total volume variation of the lung, to which we further add the deviation from a target carbon dioxide arterial partial pressure. In the present study, the stereotypical scenario appears to be a piecewise exponential one, minimizing a weighted linear combination of the three mentioned quantities, underlining the role of carbon dioxide captors, lung distension together with low effort in the breathing scenario selection. The proposed 1D system could then further be adapted to model pathologies such as asthma, emphysema, or fibrosis and understand their impact on breathing patterns, output data, and possible minimizing criteria. It could also be useful to explore the effect of mechanical ventilation and optimize the delivered applied pressure by solving a well-chosen optimal control problem.

Appendix A. Numerical data

Physiological model parameters	**Normal breathing values**	**References**
Elastance (E)	$4\,\mathrm{cmH_2O \cdot L^{-1}}$	[20, 16]
Resistance (R)	$2\,\mathrm{cmH_2O \cdot s \cdot L^{-1}}$	[20, 49]
Functional Residual Capacity (V_{FRC})	2.5 L	[20, 22]
Reduced atmospheric pressure (P_{atm})	713 mmHg	[16]
Diffusion coefficient of O_2 in air (D_{O_2})	$0.2\,\mathrm{cm^2 \cdot s^{-1}}$	[25]
Diffusion coefficient of CO_2 in air (D_{CO_2})	$0.14\,\mathrm{cm^2 \cdot s^{-1}}$	[25]
Mole fraction in fresh air for O_2 ($\chi_{\bar{O}_2}$)	21%	[16]
Mole fraction in fresh air for CO_2 ($\chi_{\bar{C}O_2}$)	0.04%	[16]
Membrane diffusing capacity of O_2 (D_{m,O_2})	$21\,\mathrm{mL \cdot min^{-1} \cdot mmHg^{-1}}$	[16]
Membrane diffusing capacity of CO_2 (D_{m,CO_2})	$420\,\mathrm{mL \cdot min^{-1} \cdot mmHg^{-1}}$	[16]
Capillary volume (V_c)	70 mL	[16, 49]
Transit time of red blood cells in V_c (τ_b)	0.75 s	[49]
Pressure of O_2 in deoxygenated blood (P_{v,O_2})	40 mmHg	[16]
Pressure of CO_2 in deoxygenated blood (P_{v,CO_2})	45 mmHg	[16]
Pressure of O_2 at 50% saturation (P_{50})	26 mmHg	[47, 11]

Table 14. Parameters used in the reference case (healthy subject at rest). They are used by default in all the simulations, unless otherwise stated.

References

[1] A. Albanese, L. Cheng, M. Ursino, and N. W. Chbat. An integrated mathematical model of the human cardiopulmonary system: model development. *American Journal of Physiology-Heart and Circulatory Physiology*, 310(7):H899–H921, 2016. PMID: 26683899.

[2] L. Baffico, C. Grandmont, and B. Maury. Multiscale modeling if the respiratory tract. *Mathematical Models and Methods in Applied Sciences*, 20(01):59–93, 2010.

[3] J. H. T. Bates. *Lung Mechanics: An Inverse Modeling Approach*. Cambridge University Press, Cambridge, 2009.

[4] A. Ben-Tal. Simplified models for gas exchange in the human lungs. *Journal of Theoretical Biology*, 238(2):474–495, 2006.

[5] A. Ben-Tal. Computational models for the study of heart-lung interactions in mammals. *Wiley Interdisciplinary Reviews Systems Biology and Medecine*, 4(2):163–170, 2012.

[6] L. Berger, R. Bordas, K. Burrowes, V. Grau, S. Tavener, and D. Kay. A poroelastic model coupled to a fluid network with applications in lung modelling. *International journal for numerical methods in biomedical engineering*, 32(1), 2016.

[7] L. Boudin, C. Grandmont, B. Grec, and S. Martin. A coupled model for the dynamics of gas exchanges in the human lung with Haldane and Bohr's effects. *Journal of Theoretical Biology*, 573:111590, 2023.

[8] R. M. Bruce. The control of ventilation during exercise: a lesson in critical thinking. *Advances in Physiology Education*, 41(4):539–547, 2017.
[9] R. Carrasco Loza, G. Villamizar RodrÃguez, and N. Medel FernÃ¡ndez. Ventilator-induced lung injury (vili) in acute respiratory distress syndrome (ards): Volutrauma and molecular effects. *The Open Respiratory Medecine Journal*, 9:112–119, 2015.
[10] L. Cheng, O. Ivanova, H.-H. Fan, and M. C. K. Khoo. An integrative model of respiratory and cardiovascular control in sleep-disordered breathing. *Respiratory Physiology & Neurobiology*, 174(1):4–28, Nov. 2010.
[11] J. A. Collins, A. Rudenski, J. Gibson, L. Howard, and R. O'Driscoll. Relating oxygen partial pressure, saturation and content : the haemoglobin-oxygen dissociation curve. *European Respiratory Society Breathe*, 11(3):194–201, 2015.
[12] L. de Rochefort, L. Vial, R. Fodil, X. Maître, B. Louis, D. Isabey, G. Caillibotte, M. Thiriet, J. Bittoun, E. Durand, and G. Sbirlea-Apiou. In vitro validation of computational fluid dynamic simulation in human proximal airways with hyperpolarized 3he magnetic resonance phase-contrast velocimetry. *Journal of Applied Physiology*, 102(5):2012–2023, 2007. PMID: 17289906.
[13] J. A. Dempsey, A. La Gerche, and J. H. Hull. Is the healthy respiratory system built just right, overbuilt, or underbuilt to meet the demands imposed by exercise? *Journal of Applied Physiology*, 129(6):1235–1256, 1985.
[14] T. Gemci, V. Ponyavin, Y. Chen, H. Chen, and R. Collins. Computational model of airflow in upper 17 generations of human respiratory tract. *Journal of Biomechanics*, 41(9):2047–2054, 2008.
[15] F. S. Grodins, J. Buell, and A. J. Bart. Mathematical analysis and digital simulation of the respiratory control system. *Journal of Applied Physiology*, 22(2):260–276, Feb. 1967.
[16] A. C. Guyton and J. E. Hall. *Textbook of Medical Physiology*. Elsevier Saunders, Philadelphia, 11th edition, 2006.
[17] R. P. Hämäläinen and A. A. Viljanen. Modelling the respiratory airflow pattern by optimization criteria. *Biological Cybernetics*, 29(3):143–149, 1978.
[18] M. Ismail, A. Comerford, and W. Wall. Coupled and reduced dimensional modeling of respiratory mechanics during spontaneous breathing. *International Journal for Numerical Methods in Biomedical Engineering*, 29(11):1285–1305, 2013.
[19] F. Jiang, T. Hirano, C. Liang, G. Zhang, K. Matsunaga, and X. Chen. Multi-scale simulations of pulmonary airflow based on a coupled 3d-1d-0d model. *Computers in Biology and Medicine*, 171:108150, 2024.
[20] A. T. Johnson. *Biomechanics and Exercise Physiology: Quantitative Modeling*. CRC Press, Boca Raton, 2007.
[21] C. Karamaoun, A. Van Muylem, and B. Haut. Modeling of the nitric oxide transport in the human lungs. *Frontiers in Physiology*, 7:255, 2016.
[22] B. M. Koeppen and B. A. Stanton, editors. *Berne & Levy Physiology*. Elsevier, Philadelphia, 7th edition, 2018.
[23] H. Malte and G. Lykkeboe. The bohr/haldane effect: a model-based uncovering of the full extent of its impact on o2 delivery to and co2 removal from tissues. *Journal of Applied Physiology*, 125:916–922, 2018.
[24] S. Martin and B. Maury. Modeling of the oxygen transfer in the respiratory process. *ESAIM: Mathematical Modelling and Numerical Analysis*, 47(4):935–960, 2013.
[25] B. Mauroy. *Hydrodynamique dans le poumon, relations entre flux et géométries*. PhD thesis, École normale supérieure de Cachan, Paris, 2004.
[26] B. Maury. *The Respiratory System in Equations*. Number 7 in MS&A - Modeling, Simulations & Applications. Springer-Verlag, 2013.
[27] J. Mead. Control of respiratory frequency. *Journal of Applied Physiology*, 15(3):325–336, 1960.
[28] C. Ngo, S. Dahlmanns, T. Vollmer, B. Misgeld, and S. Leonhardt. An object-oriented computational model to study cardiopulmonary hemodynamic interactions in humans. *Computer Methods and Programs in Biomedicine*, 159:167–183, 2018.
[29] F. Noël and B. Mauroy. Interplay between optimal ventilation and gas transport in a model of the human lung. *Frontiers in Physiology*, 10:488, 2019.
[30] J. M. Oakes, S. C. Shadden, C. Grandmont, and I. E. Vignon-Clementel. Aerosol transport throughout inspiration and expiration in the pulmonary airways. *International Journal for Numerical Methods in Biomedical Engineering*, 33(9):e2847, 2017.
[31] A. B. Otis, W. O. Fenn, and H. Rahn. Mechanics of breathing in man. *Journal of Applied Physiology*, 2(11):592–607, 1950.
[32] M. Paiva and L. Engel. Influence of bronchial asymmetry on cardiogenic gas mixing in the lung. *Respiration Physiology*, 49(3):325–338, 1982.
[33] M. Paiva and L. A. Engel. Model analysis of gas distribution within human lung acinus. *Journal of Applied Physiology: respiratory, environmental and exercise physiology*, 56(2):418–425, 1984.
[34] C. Patte, M. Genet, and D. Chapelle. A quasi-static poromechanical model of the lungs. *Biomechanics and Modeling in Mechanobiology*, 21(2):527–551, 2022.

[35] N. Pozin, S. Montesantos, I. Katz, M. Pichelin, I. Vignon-Clementel, and C. Grandmont. A tree-parenchyma coupled model for lung ventilation simulation. *International Journal for Numerical Methods in Biomedical Engineering*, 33(11):e2873, 2017. e2873 CNM-Sep-16-0190.R1.
[36] O. Raabe. *Tracheobronchial geometry-human, dog, rat, hamster*. 1976.
[37] B. Sapoval and M. Filoche. Role of diffusion screening in pulmonary diseases. *Advances in Experimental Medicine and Biology*, 605:173–178, 2008.
[38] B. Sapoval, M. Filoche, and E. R. Weibel. Smaller is better − but not too small: A physical scale for the design of the mammalian pulmonary acinus. *Proceedings of the National Academy of Sciences of the United States of America*, 99:10411–10416, 2002.
[39] K. B. Saunders, H. N. Bali, and E. R. C. A breathing model of the respiratory system: The controlled system. *Journal of Theoretical Biology*, 84(1):135–161, May 1980.
[40] J. D. Schwardt, S. R. Gobran, G. R. Neufeld, S. J. Aukburg, and S. P. W. Sensitivity of co2 washout to changes in acinar structure in a single-path model of lung airways. *Annals of Biomedical Engineering*, 19(6):679–697, 1991.
[41] T. T. Soong, P. Nicolaides, C. P. Yu, and S. C. Soong. A statistical description of the human tracheobronchial tree geometry. *Respiration Physiology*, 37:161–172, 1979.
[42] A. J. Swan, A. R. Clark, and M. H. Tawhai. A computational model of the topographic distribution of ventilation in healthy human lungs. *Journal of Theoretical Biology*, 300:222–231, 2012.
[43] A. J. Swan and M. H. Tawhai. Evidence for minimal oxygen heterogeneity in the healthy human pulmonary acinus. *Journal of Applied Physiology*, 110(2):528–537, 2011.
[44] V. Tedjasaputra, M. M. Bouwsema, and S. M. K. Effect of aerobic fitness on capillary blood volume and diffusing membrane capacity responses to exercise. *The Journal of Physiology*, 594(15):4359–4370, 2016.
[45] A. Van Muylem, C. Noël, and M. Paiva. Modeling of impact of gas molecular diffusion on nitric oxide expired profile. *Journal of Applied Physiology (Bethesda, Md.: 1985)*, 94(1):119–127, Jan. 2003.
[46] P. D. Wagner. Ventilation-perfusion matching during exercise. *Chest*, 101(5):192S–198S, 1992.
[47] K. Webb, P. Dominelli, S. Baker, S. Klassen, M. Joyner, J. Senefeld, and C. Wiggins. Influence of high hemoglobin-oxygen affinity on humans during hypoxia. *Frontiers in Physiology*, 12, 01 2022.
[48] E. R. Weibel. *Morphometry of the Human Lung*. Academic Press, New York, 1963.
[49] J. B. West. *Respiratory Physiology: The Essentials*. Lippincott Williams and Wilkins, Philadelphia, 9th edition, 2011.

S.M. benefited from the support of the France 2030 program through the IdEx Université Paris Cité (ANR 18 IDEX 0001).

[1] LJLL, Sorbonne Université, CNRS, & Inria Paris, France, & ULB, Belgium
Email address: celine.grandmont@inria.fr

[2]TIPS, Université libre de Bruxelles, Brussels, Belgium
Email address: cyril.karamaoun@ulb.be

[3]MAP5, Université Paris Cité, CNRS, F-75006 Paris - France
Email address: sebastien.martin@u-paris.fr

[4]LJLL, Sorbonne Université, CNRS, & Inria Paris
Email address: frederique.noel@sorbonne-universite.fr